



CERN-EP-2023-242
 LHCb-PAPER-2023-022
 March 14, 2024

Measurement of J/ψ -pair production in pp collisions at $\sqrt{s} = 13$ TeV and study of gluon transverse-momentum dependent PDFs

LHCb collaboration[†]

Abstract

The production cross-section of J/ψ pairs in proton-proton collisions at a centre-of-mass energy of $\sqrt{s} = 13$ TeV is measured using a data sample corresponding to an integrated luminosity of 4.2 fb^{-1} collected by the LHCb experiment. The measurement is performed with both J/ψ mesons in the transverse momentum range $0 < p_T < 14 \text{ GeV}/c$ and rapidity range $2.0 < y < 4.5$. The cross-section of this process is measured to be $16.36 \pm 0.28 \text{ (stat)} \pm 0.88 \text{ (syst)} \text{ nb}$. The contributions from single-parton scattering and double-parton scattering are separated based on the dependence of the cross-section on the absolute rapidity difference Δy between the two J/ψ mesons. The effective cross-section of double-parton scattering is measured to be $\sigma_{\text{eff}} = 13.1 \pm 1.8 \text{ (stat)} \pm 2.3 \text{ (syst)} \text{ mb}$. The distribution of the azimuthal angle ϕ_{CS} of one of the J/ψ mesons in the Collins-Soper frame and the p_T -spectrum of the J/ψ pairs are also measured for the study of the gluon transverse-momentum dependent distributions inside protons. The extracted values of $\langle \cos 2\phi_{\text{CS}} \rangle$ and $\langle \cos 4\phi_{\text{CS}} \rangle$ are consistent with zero, but the presence of azimuthal asymmetry at a few percent level is allowed.

Published in JHEP 03 (2024) 088

© 2024 CERN for the benefit of the LHCb collaboration. CC BY 4.0 licence.

[†]Authors are listed at the end of this paper.

1 Introduction

In the Standard Model (SM) of particle physics, the strong interaction is described by quantum chromodynamics (QCD). In the low-energy regime, the QCD coupling constant evolves to be so large that perturbation theory is not valid any more. The details of how the fundamental quarks and gluons are distributed inside hadrons and dynamically generate the hadron mass and spin are still largely unknown. As a building block of the physical world, the proton lies at the forefront of hadron structure studies. Moreover, the knowledge of the partonic structure of the proton is an essential input to the majority of measurements at hadron colliders, including searches for physics beyond the SM, among which the W -mass measurement is a typical example [1–4].

In the past, the internal structure of the proton was mainly studied in terms of one-dimensional parton distribution functions (PDFs) that parameterise the longitudinal momentum fraction (usually denoted x) distributions of partons inside the proton. Recently, significant progress has been made in constructing the theoretical framework for transverse-momentum dependent parton distribution functions (TMDs) [5–7], leading to a more comprehensive understanding of the proton structure. The quark TMDs have been studied through semi-inclusive deep-inelastic scattering and Drell-Yan measurements at HERMES, COMPASS and E866/NuSea experiments, and at a series of experiments at JLab [8–13]. The gluon TMDs, however, are much less known, so probing gluon TMDs is one of the major objectives of future experimental facilities like the Electron Ion Collider (EIC) [14], LHCSpin [15] and LHC fixed-target experiments [16]. In unpolarised protons, the gluon TMDs can be parameterised at leading twist using two TMDs [5]: the distribution of unpolarised gluons $f_1^g(x, k_T^2, \mu)$ and that of linearly polarised gluons $h_1^{\perp g}(x, k_T^2, \mu)$, in which k_T is the gluon transverse momentum and μ is the factorisation scale. In particular, the knowledge on the $h_1^{\perp g}(x, k_T^2, \mu)$ function is still very limited. The production of J/ψ pairs in proton-proton (pp) collisions through single-parton scattering (SPS) has been proposed as the golden channel to probe gluon TMDs, in which the presence of linearly polarised gluons will lead to azimuthal asymmetries at the percent level [17, 18]. The transverse momentum (p_T) spectrum of J/ψ pairs also encodes information on $f_1^g(x, k_T^2, \mu)$. In fact, the differential production cross-section of J/ψ pairs as a function of p_T measured by the LHCb experiment using the 2015 data was used to perform the first fit of $f_1^g(x, k_T^2, \mu)$ and obtain $\langle k_T^2 \rangle$ at an effective factorisation scale [17, 19].

Quarkonium production is also one of the best tools to study hadronisation. The non-relativistic QCD (NRQCD) model provides the most successful description of quarkonium production so far, but it still can not describe coherently the production and polarisation of various quarkonium states measured in different collisions [20–23]. The SPS production of J/ψ pairs (also referred to as di- J/ψ hereafter) can add valuable information to solve this puzzle [24–27]. In addition to SPS, quarkonium pairs can be produced through double-parton scattering (DPS) [28]. It is a process of great interest, which has been widely studied by many experiments via various reactions [29–42]. It can be used, for instance, to reveal the profile and correlation of partons inside the proton, which are encoded in a characteristic parameter of DPS called effective cross-section, denoted as σ_{eff} [43–45]. The contribution from DPS can be estimated according to the formula [43–45]

$$\sigma_{\text{di-}J/\psi}^{\text{DPS}} = \frac{1}{2} \frac{\sigma_{J/\psi}^2}{\sigma_{\text{eff}}}, \quad (1)$$

where $\sigma_{J/\psi}$ is the prompt J/ψ meson production cross-section, and the factor one-half accounts for the two identical particles in the final state. The effective cross-section σ_{eff} characterises the transverse overlap area between the interacting partons.

In this paper, the J/ψ -pair production cross-section in pp collisions at a centre-of-mass energy of $\sqrt{s} = 13$ TeV is measured for J/ψ mesons with $p_T < 14$ GeV/ c and rapidity $2.0 < y < 4.5$ using a subset of data collected by the LHCb experiment from 2016 to 2018 with specific trigger requirements, corresponding to an integrated luminosity of 4.2 fb^{-1} . The azimuthal asymmetry of J/ψ pairs is measured to probe the TMD function $h_1^{\perp g}(x, k_T^2, \mu)$, presenting the first experimental measurement of linear polarisation of gluons inside unpolarised protons. The p_T spectrum of the J/ψ pairs is measured in intervals of J/ψ -pair rapidity and mass, which will help to extract $f_1^g(x, k_T^2, \mu)$ with the TMD evolution effect considered [18]. Updates of the differential production cross-sections given in the previous LHCb measurement using data with a luminosity of about 0.3 fb^{-1} at $\sqrt{s} = 13$ TeV [19] are also provided, with the SPS and DPS contributions separated without dependence on any specific SPS production model.

2 Detector and simulation

The LHCb detector [46, 47] is a single-arm forward spectrometer covering the pseudorapidity range $2 < \eta < 5$, designed for the study of particles containing b - or c -quarks. The detector includes a high-precision tracking system consisting of a silicon-strip vertex detector surrounding the pp interaction region, a large-area silicon-strip detector located upstream of a dipole magnet with a bending power of about 4 Tm, and three stations of silicon-strip detectors and straw drift tubes placed downstream of the magnet. The tracking system provides a measurement of the momentum, p , of charged particles with a relative uncertainty that varies from 0.5% at low momentum to 1.0% at 200 GeV/ c . The minimum distance of a track to a primary pp collision vertex (PV), the impact parameter (IP), is measured with a resolution of $(15 + 29/p_T) \mu\text{m}$, where p_T is in GeV/ c . Different types of charged hadrons are distinguished using information from two ring-imaging Cherenkov detectors. Photons, electrons and hadrons are identified by a calorimeter system consisting of scintillating-pad and preshower detectors, an electromagnetic and a hadronic calorimeter. Muons are identified by a system composed of alternating layers of iron and multiwire proportional chambers.

Simulated samples of J/ψ mesons are produced to study the expected behaviour of experimental signals and determine the detection efficiencies. The pp collisions are modelled using PYTHIA [48, 49] with a specific LHCb configuration [50]. In the PYTHIA model, J/ψ mesons are not polarised, and the leading order colour-singlet and colour-octet contributions [50, 51] are included in prompt J/ψ meson production. Decays of unstable particles are described by EVTGEN [52] with QED final-state radiation handled by PHOTOS [53]. The interactions of the generated particles with the detector are modelled using the GEANT4 toolkit [54, 55] as described in Ref. [56].

3 Candidate selection

The di- J/ψ candidates are reconstructed through the $J/\psi \rightarrow \mu^+ \mu^-$ decays. The online event selection is performed by a trigger [57], which consists of a hardware stage (L0),

based on information from the calorimeter and muon systems, followed by a two-step software stage (HLT1 and HLT2), which applies a full event reconstruction. At least one J/ψ meson is required to fulfil the selection criteria of the L0 and HLT1 triggers. The L0 trigger selects two muons with the product of their transverse momenta larger than 1.3^2 , 1.5^2 or 1.8^2 (GeV/c) 2 , depending on the data taking period. The HLT1 trigger requires two good-quality tracks with $p_T > 0.3 \text{ GeV}/c$ and $p > 6 \text{ GeV}/c$, that are loosely identified as muons and form a J/ψ candidate with an invariant mass $m_{\mu^+\mu^-} > 2.7 \text{ GeV}/c^2$ or $2.9 \text{ GeV}/c^2$, depending on the data taking period. The HLT2 trigger requires both $\mu^+\mu^-$ pairs to form a good vertex and have an invariant mass $m_{\mu^+\mu^-}$ within $120 \text{ MeV}/c^2$ of the world-average value of the J/ψ mass [58]. Offline selections are applied to the di- J/ψ candidates to further reduce the combinatorial background. All the four muon tracks are required to have $1.9 < \eta < 4.9$, $p_T > 0.65 \text{ GeV}/c$ and $p > 3 \text{ GeV}/c$.

In pp collisions, J/ψ mesons can be produced promptly at the PV, or in the decays of beauty hadrons. The nonprompt contributions with the J/ψ mesons originating from the decay vertices of beauty hadrons, which are typically separated from the PV, need to be subtracted in this analysis. The prompt and nonprompt J/ψ mesons can be distinguished by exploiting the pseudoproper time [59]

$$t_z = \frac{z_{J/\psi} - z_{\text{PV}}}{p_z} \times m_{J/\psi}, \quad (2)$$

where $z_{J/\psi}$ and z_{PV} are the positions of the J/ψ meson decay vertex and its associated PV along the beam axis z , p_z the component of the J/ψ momentum along the z -axis, and $m_{J/\psi}$ the world-average value of the J/ψ mass [58]. The uncertainty σ_{t_z} is calculated by combining the uncertainties on $z_{J/\psi}$ and z_{PV} since the uncertainty on p_z is negligible in comparison. Candidates with both J/ψ mesons having $-2 < t_z < 10 \text{ ps}$ and $\sigma_{t_z} < 0.3 \text{ ps}$ are retained. Finally, the four muon tracks are required to originate from the same PV, which reduces to a negligible level the number of candidates with the two J/ψ mesons originating from different pp interactions.

4 Cross-section determination

The di- J/ψ production cross-section is calculated as

$$\sigma_{\text{di-}J/\psi} = \frac{N^{\text{corr}}}{\mathcal{L} \times \mathcal{B}^2(J/\psi \rightarrow \mu^+\mu^-)}, \quad (3)$$

where N^{corr} is the signal yield after detection efficiency corrections, $\mathcal{L} = 4.18 \pm 0.08 \text{ fb}^{-1}$ is the integrated luminosity measured using the van der Meer scan method [60], and $\mathcal{B}(J/\psi \rightarrow \mu^+\mu^-) = (5.961 \pm 0.033)\%$ [58] is the branching fraction of the $J/\psi \rightarrow \mu^+\mu^-$ decay.

The di- J/ψ signals are extracted by performing a two-dimensional (2D) unbinned extended maximum likelihood fit to the distribution of the two J/ψ meson masses, $(m_{\mu_1^+\mu_1^-}, m_{\mu_2^+\mu_2^-})$. The two $J/\psi \rightarrow \mu^+\mu^-$ decays are labelled as $J/\psi_1 \rightarrow \mu_1^+\mu_1^-$ and $J/\psi_2 \rightarrow \mu_2^+\mu_2^-$ at random. There are four components of the 2D mass distribution: a signal di- J/ψ decay, a true $J/\psi_1 \rightarrow \mu_1^+\mu_1^-$ decay with a dimuon background $\mu_2^+\mu_2^-$, a dimuon background $\mu_1^+\mu_1^-$ with a true $J/\psi_2 \rightarrow \mu_2^+\mu_2^-$ decay, and the association of two combinatorial dimuon backgrounds. The second and the third components have the equal fraction because the

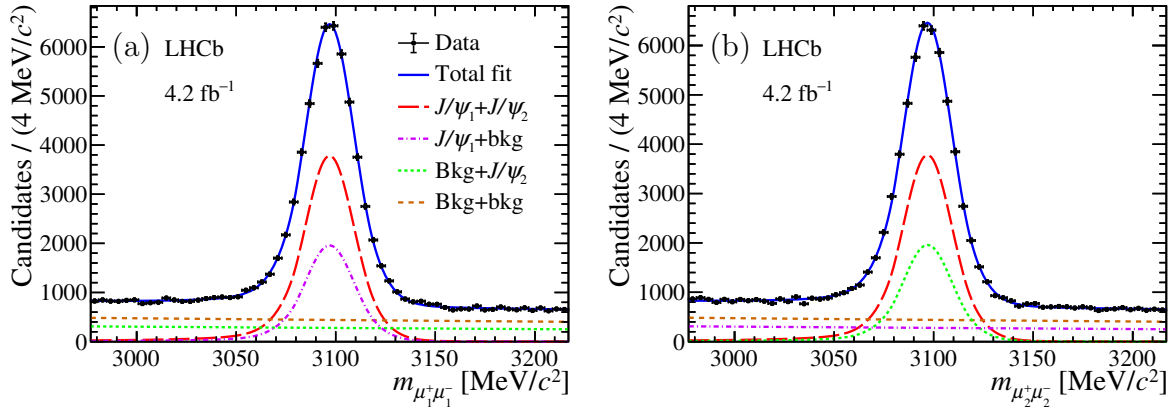


Figure 1: Invariant mass distributions of two $\mu^+\mu^-$ pairs (a) $m_{\mu_1^+\mu_1^-}$ and (b) $m_{\mu_2^+\mu_2^-}$ for di- J/ψ candidates together with the projections of the two-dimensional fit.

mass distributions of the two J/ψ mesons are symmetric. For the mass distribution of each J/ψ meson, the signal component is described by the sum of a double-sided Crystal Ball (DSCB) function [61] with asymmetric tails and a Gaussian function with a common mean value but different widths. The tail parameters of the DSCB function, the fraction of the DSCB function and the ratio between the two widths are fixed from simulation. Only the common mean value and the width of the DSCB function are left as free parameters. The distribution of the combinatorial dimuon background component is modelled with an exponential function. Figure 1 shows the mass distributions for the two $\mu^+\mu^-$ pairs and the projections of the fit result on $m_{\mu_1^+\mu_1^-}$ and $m_{\mu_2^+\mu_2^-}$.

The subtraction of the nonprompt contributions is performed using a 2D unbinned extended maximum likelihood fit to the t_z distribution of each J/ψ meson of the di- J/ψ signals with backgrounds subtracted using the *sPlot* method [62], taking $m_{\mu_1^+\mu_1^-}$ and $m_{\mu_2^+\mu_2^-}$ as the discriminating variables. The true t_z distribution of prompt J/ψ mesons is expected to follow a Dirac delta function $\delta(t_z)$, while that of nonprompt J/ψ mesons should follow an exponential function. These are convolved with the sum of two Gaussian functions to model the detector resolution. The parameters of the resolution function are free parameters in the fit. A third component describes candidates with incorrectly associated PVs and is modelled using a binned histogram extracted from data by calculating t_z with one J/ψ meson associated to the closest PV in the next event. Figure 2 shows the t_z distributions for the two J/ψ mesons and the projections of the 2D fit result on t_z^{J/ψ_1} and t_z^{J/ψ_2} . The yield of prompt di- J/ψ signal is $(2.187 \pm 0.020) \times 10^4$, accounting for around 68% of the total di- J/ψ signal yield.

Since the kinematic distribution of the di- J/ψ signal is unknown a priori, the efficiency correction is performed on a per-event basis as

$$N^{\text{corr}} = \sum_i \frac{\omega_i}{\varepsilon_i^{\text{tot}}}, \quad (4)$$

where i is the event index, ω_i is the *sPlot* weight corresponding to the component of prompt di- J/ψ signal, and $\varepsilon_i^{\text{tot}}$ is the total efficiency for each candidate. Since no information related to the correlation of the two J/ψ mesons is used during the reconstruction and selection, the detection efficiency of the di- J/ψ candidate can be factorised into that of the

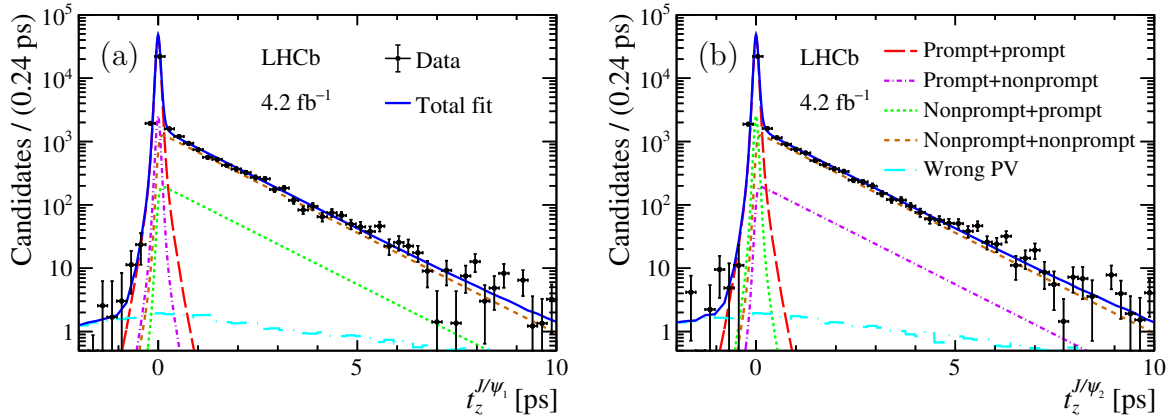


Figure 2: Distributions of (a) t_z^{J/ψ_1} and (b) t_z^{J/ψ_2} for di- J/ψ signals with backgrounds subtracted. The projections of the fit result are overlaid.

two J/ψ mesons, which are determined from simulation as functions of the p_T and y of the J/ψ mesons. The efficiency $\varepsilon_i^{\text{tot}}$ is the product of the geometrical acceptance $\varepsilon_i^{\text{acc}}$, the reconstruction and selection efficiency $\varepsilon_i^{\text{rec\&sel}}$, the particle identification (PID) efficiency $\varepsilon_i^{\text{PID}}$, and the trigger efficiency $\varepsilon_i^{\text{trig}}$, giving

$$\varepsilon_i^{\text{tot}} = \varepsilon_i^{\text{acc}} \times \varepsilon_i^{\text{rec\&sel}} \times \varepsilon_i^{\text{PID}} \times \varepsilon_i^{\text{trig}}. \quad (5)$$

The efficiencies $\varepsilon_i^{\text{acc}}$, $\varepsilon_i^{\text{rec\&sel}}$ and $\varepsilon_i^{\text{PID}}$ of a di- J/ψ candidate factorise as the product of that of the two J/ψ mesons, *i.e.*

$$\varepsilon_i(\text{di-}J/\psi) = \varepsilon_i(J/\psi_1) \times \varepsilon_i(J/\psi_2), \quad (6)$$

while the trigger efficiency $\varepsilon_i^{\text{trig}}$ of each di- J/ψ candidate factorises as

$$\varepsilon_i^{\text{trig}}(\text{di-}J/\psi) = 1 - (1 - \varepsilon_i^{\text{L0\&HLT1}}(J/\psi_1)) (1 - \varepsilon_i^{\text{L0\&HLT1}}(J/\psi_2)), \quad (7)$$

where $\varepsilon_i^{\text{L0\&HLT1}}$ is the L0 and HLT1 trigger efficiency. The offline selection criterion is tighter than the HLT2 requirements, making the HLT2 trigger fully efficient with respect to offline selected candidates. The track reconstruction efficiency, which is part of $\varepsilon_i^{\text{rec\&sel}}$, and the PID efficiency $\varepsilon_i^{\text{PID}}$ are calibrated using data-driven techniques to avoid known discrepancies between the simulation and data [63, 64]. With the detection efficiency corrected, the signal yield is determined to be $N^{\text{corr}} = (2.43 \pm 0.04) \times 10^5$, where the statistical uncertainty is verified by a bootstrapping approach [65].

5 Systematic uncertainties

Systematic uncertainties are studied and summarised in Table 1. The uncertainty due to imperfect modelling of the J/ψ mass distribution is estimated by using an alternative function for the J/ψ signal component in the fit. A model derived from the simulation using kernel density estimation [66] is used instead. The relative variation of the extracted signal yield is 1.7%, which is taken as the systematic uncertainty. The uncertainty on the determination of the nonprompt contribution is evaluated by using an alternative variable

for the discrimination. The $\log(\chi^2_{\text{IP}})$ of the J/ψ mesons is used instead of t_z , where χ^2_{IP} is defined as the difference in the vertex-fit χ^2 of the associated PV reconstructed with and without the J/ψ meson under consideration. The relative deviation from the nominal result, 2.4%, is taken as the systematic uncertainty. For the measurement of differential cross-sections, these two uncertainties are taken as common to all kinematic intervals.

For a very small fraction of the di- J/ψ candidates, the J/ψ mesons may be associated to a wrong PV in two cases. In the first, the true PV is reconstructed but one of the two J/ψ candidates is associated to a wrong PV, while in the second the true PV is not reconstructed and both J/ψ mesons are associated to the same reconstructed PV in this event. For the first case, two J/ψ mesons are associated to different PVs and thus are rejected by the selection. The fraction of the first case is estimated using a simulated sample of $\Upsilon(1S) \rightarrow J/\psi J/\psi \gamma$ decays to be $(0.65 \pm 0.02)\%$. The second case is the wrong-PV component in the 2D t_z fit, and its fraction is $(0.16 \pm 0.08)\%$. The total fraction of wrong-PV candidates adds up to 0.8%, which is taken as the systematic uncertainty. For the differential cross-sections, the fraction is studied in several intervals of the di- J/ψ rapidities using the same method. The maximum fraction, 1.5%, is conservatively taken as the uncertainty common to all kinematic intervals.

The uncertainty due to the finite sample size of the calibration samples used for efficiency determination is propagated to the final result using pseudoexperiments. It is determined to be 0.2% and varies up to 1.1% depending on the kinematic intervals for the differential cross-sections. The binning scheme that is used to determine the efficiencies could bias the signal yield N^{corr} . For the PID efficiency, this effect is estimated by varying the binning schemes of the PID calibration sample. For the remaining efficiency terms, an alternative kernel density estimation approach [66] is used to determine the efficiencies as functions of $(p_T^{J/\psi}, y_{J/\psi})$. The relative difference in the cross-sections between the default and alternative approaches is 1.5% and quoted as the systematic uncertainty. For the measurement of differential cross-sections, it varies up to 6.6% depending on the kinematic intervals. The uncertainty on the track reconstruction efficiency consists of the statistical uncertainty due to the limited size of the calibration samples, which is estimated from pseudoexperiments to be 1.2% for di- J/ψ candidates, and the uncertainty due to the dependence of calibration factors on the event multiplicity, which is 0.8% per track. The two terms are added in quadrature to 3.4%. For the differential cross-sections, the first term varies up to 3.8%, while the second is considered to be common to all kinematic intervals. The trigger efficiency determined from the simulation is validated with the prompt J/ψ data, using a subset of events that fulfil the trigger requirement with the J/ψ signals excluded [57]. The relative difference in the di- J/ψ cross-section calculated using the trigger efficiencies from the data and the simulation is 0.7%, and is taken as the systematic uncertainty. For the differential cross-sections, the uncertainty on the trigger efficiency varies up to 7.9% depending on the kinematic intervals.

The uncertainty on the $J/\psi \rightarrow \mu^+ \mu^-$ branching fraction leads to an uncertainty of 1.1% on the di- J/ψ production cross-section. The relative uncertainty on the luminosity is determined to be 2.0%. With these uncertainties due to independent effects added in quadrature, the total systematic uncertainty on the di- J/ψ production cross-section is determined to be 5.4%.

Table 1: Summary of the systematic uncertainties on the measurement of the di- J/ψ production cross-section. The total systematic uncertainty is a quadratic sum of these uncertainties.

Source	Uncertainty (%)
Signal mass model	1.7
Nonprompt contribution	2.4
Wrong PV association	0.8
Calibration sample statistics	0.2
Efficiency determination	1.5
Track reconstruction efficiency	3.4
Trigger efficiency	0.7
Branching fraction	1.1
Luminosity	2.0
Total	5.4

6 Production cross-sections

The cross-section of the di- J/ψ production with both J/ψ mesons in the fiducial range $p_T < 14 \text{ GeV}/c$ and $2.0 < y < 4.5$ is measured to be

$$\sigma_{\text{di-}J/\psi} = 16.36 \pm 0.28 \text{ (stat)} \pm 0.88 \text{ (syst)} \text{ nb},$$

where the first uncertainty is statistical and the second systematic, assuming negligible polarisation of the J/ψ mesons. The detection efficiency for the J/ψ mesons depends on their polarisation. In the helicity frame, there is a strong dependence on the polarisation parameter λ_θ [67, 68]. For instance, when λ_θ is assumed to be +0.2 (−0.2) for both J/ψ mesons, the di- J/ψ production cross-section changes by +6.2% (−6.3%) evaluated from simulation.

The differential di- J/ψ production cross-section as a function of a kinematic variable u is measured as

$$\frac{d\sigma_{\text{di-}J/\psi}}{du} = \frac{\Delta N^{\text{corr}}(\text{di-}J/\psi)}{\mathcal{L} \times \mathcal{B}^2(J/\psi \rightarrow \mu^+ \mu^-) \times \Delta u}, \quad (8)$$

where ΔN^{corr} is the efficiency-corrected signal yield in an interval of the variable u , and Δu is the interval width. In this analysis the cross-sections are reported as functions of: the absolute difference in rapidity between the two J/ψ mesons Δy ; the absolute difference in the azimuthal angle ϕ , defined in the laboratory frame, between the two J/ψ mesons $\Delta\phi$; the transverse momentum asymmetry \mathcal{A}_{p_T} of the two J/ψ mesons, defined as

$$\mathcal{A}_{p_T} = \left| \frac{p_T^{J/\psi_1} - p_T^{J/\psi_2}}{p_T^{J/\psi_1} + p_T^{J/\psi_2}} \right|; \quad (9)$$

the transverse momentum $p_T^{\text{di-}J/\psi}$, rapidity $y_{\text{di-}J/\psi}$ and invariant mass $m_{\text{di-}J/\psi}$ of the di- J/ψ signals; and the transverse momentum $p_T^{J/\psi}$ and rapidity $y_{J/\psi}$ of either J/ψ meson. The binning scheme is chosen to have adequate and approximately even signal yield in each category. The differential cross-section as a function of $p_T^{J/\psi}$ ($y_{J/\psi}$) is taken as the average of the two distributions of p_T^{J/ψ_1} (y_{J/ψ_1}) and p_T^{J/ψ_2} (y_{J/ψ_2}), taking advantage of the symmetry between the two J/ψ mesons. The 2D mass fit and the 2D pseudoproper time

fit are performed independently for each kinematic interval to subtract the combinatorial backgrounds and the nonprompt contributions, respectively. The measured differential cross-sections of the di- J/ψ production are shown in Figure 3 as black data points (SPS+DPS), and summarised in Tables 2–9 in Appendix A.

7 Separation of DPS and SPS contributions

The distributions of the rapidity difference (Δy) between the two J/ψ mesons have different shapes for the SPS and DPS processes [31, 39, 69], so the DPS contribution can be extracted using the Δy distribution with a data-driven template for the DPS process. The shape of the DPS component is obtained by combining two uncorrelated J/ψ mesons whose distributions follow the measured differential production cross-section of the single prompt J/ψ [68], assuming they are both uniformly distributed over the azimuthal angle ϕ . According to the NRQCD predictions [24–27], the SPS contribution to the di- J/ψ production in the range $1.8 < \Delta y < 2.5$ is negligible. The normalisation of the DPS contribution is thus determined in this range, while the remaining contribution is assigned to SPS. For the extraction of the DPS contribution, three sources of systematic uncertainties are considered: the uncertainty due to possible SPS remnant in the $1.8 < \Delta y < 2.5$ range, which is studied by varying the Δy range for normalisation and estimated to be 3.5%; the uncertainty on the DPS template due to the binning scheme of the prompt J/ψ differential cross-sections, which is estimated to be 3.3%, determined through the relative difference between the results with and without interpolation across the intervals; the uncertainty propagated from the prompt J/ψ production cross-section, which is 1.8%. Consequently, the DPS cross-section of the di- J/ψ production with both J/ψ mesons in the fiducial range $p_T < 14 \text{ GeV}/c$ and $2.0 < y < 4.5$ is determined to be

$$\sigma_{\text{di-}J/\psi}^{\text{DPS}} = 8.6 \pm 1.2 \text{ (stat)} \pm 1.0 \text{ (syst)} \text{ nb.}$$

According to Eq. 1, the effective cross-section σ_{eff} is measured to be

$$\sigma_{\text{eff}} = \frac{1}{2} \frac{\sigma_{J/\psi}^2}{\sigma_{\text{di-}J/\psi}^{\text{DPS}}} = 13.1 \pm 1.8 \text{ (stat)} \pm 2.3 \text{ (syst)} \text{ mb,}$$

where the prompt J/ψ production cross-section $\sigma_{J/\psi}$ in the range $0 < p_T < 14 \text{ GeV}/c$ and $2.0 < y < 4.5$ is $\sigma_{J/\psi} = 15.03 \pm 0.03 \text{ (stat)} \pm 0.94 \text{ (syst)} \mu\text{b}$ [68], and the systematic uncertainties on $\sigma_{\text{di-}J/\psi}^{\text{DPS}}$ and $\sigma_{J/\psi}$ are treated as uncorrelated. The σ_{eff} result is compatible with existing measurements from different experiments in pp and $p\bar{p}$ collisions, as shown in Figure 4. With the DPS cross-section subtracted, the SPS cross-section of di- J/ψ production with both J/ψ mesons in the fiducial range $p_T < 14 \text{ GeV}/c$ and $2.0 < y < 4.5$ is determined to be

$$\sigma_{\text{di-}J/\psi}^{\text{SPS}} = 7.9 \pm 1.2 \text{ (stat)} \pm 1.1 \text{ (syst)} \text{ nb.}$$

The differential di- J/ψ production cross-sections are shown in Figure 3 with the DPS and SPS contributions separated. The differential cross-sections for DPS are obtained by normalising the data-driven DPS template to the total DPS cross-section in the fiducial range, and the uncertainties are propagated from the total DPS cross-section. The extracted differential SPS cross-sections are listed in Tables 10–17 in Appendix A. By definition the SPS and DPS components are anti-correlated. In general, the difference

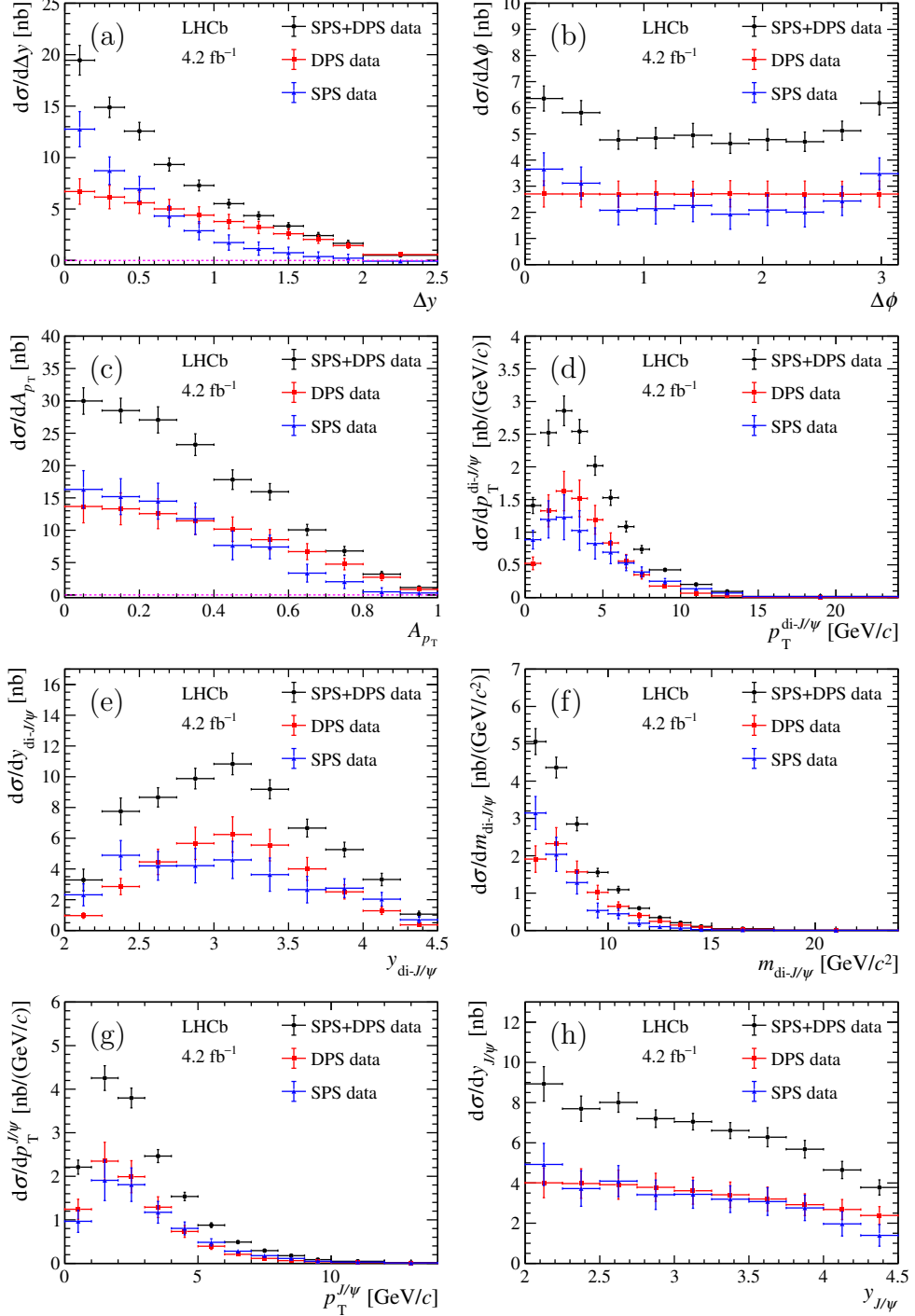


Figure 3: Differential cross-section of di- J/ψ production for SPS+DPS, DPS and SPS as a function of (a) Δy , (b) $\Delta\phi$, (c) A_{p_T} , (d) $p_T^{\text{di-}J/\psi}$, (e) $y_{\text{di-}J/\psi}$, (f) $m_{\text{di-}J/\psi}$, (g) $p_T^{J/\psi}$ and (h) $y_{J/\psi}$. The error bars represent the statistical and systematic uncertainties added in quadrature. The purple dashed lines in (a) and (c) indicate the baseline of zero.

in distributions between DPS and SPS is due to the fact that the kinematics of two J/ψ mesons are uncorrelated for DPS while correlated for SPS. Figure 3(a) shows that the Δy distribution for the DPS process is wider than that for the SPS process. As shown

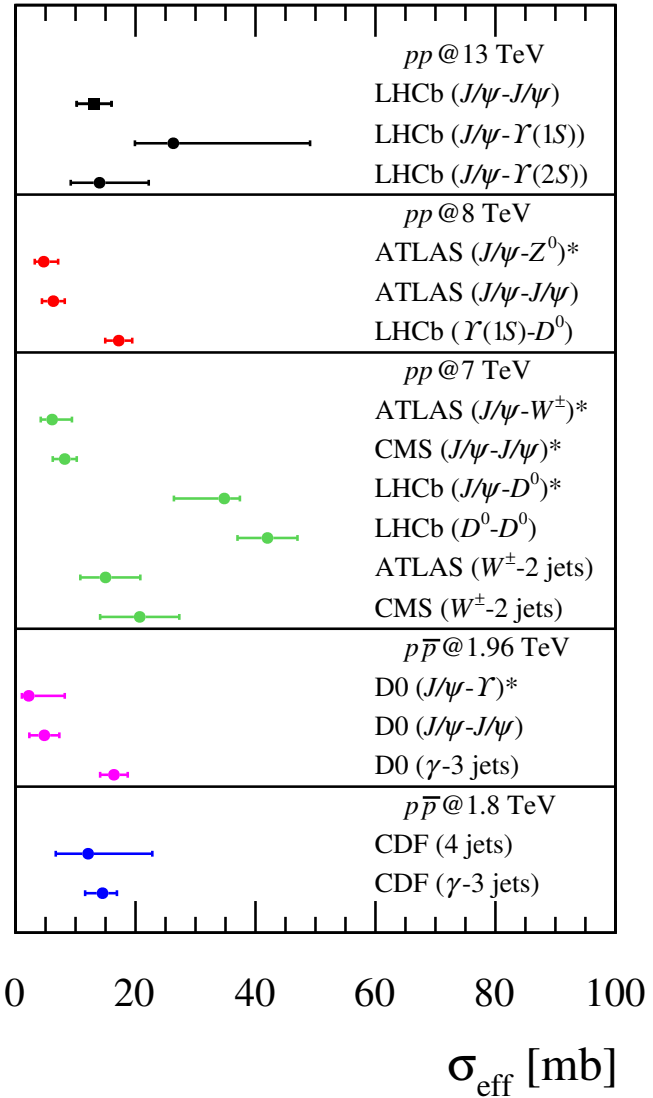


Figure 4: Summary of σ_{eff} measurements in pp or $p\bar{p}$ collisions [29–42]. The legend entries marked with an asterisk are taken from a third-party calculation based on the original experimental result [28, 70–73].

in Figure 3(b), the $\Delta\phi$ distribution for SPS peaks at $\Delta\phi = 0$ and π , while the DPS distribution is flat because two uncorrelated J/ψ mesons are assumed to be uniformly distributed over the angle ϕ in the data-driven template. The distributions of \mathcal{A}_{p_T} and $m_{\text{di-}J/\psi}$ for DPS are both slightly wider than those for SPS, as shown in Figures 3(c) and 3(f).

The no-loop next-to-leading-order colour-singlet (NLO* CS) predictions [74] of the di- J/ψ production via SPS are obtained from HELAC-Onia [75, 76], an automatic matrix element generator for heavy quarkonium physics. The measured SPS differential cross-

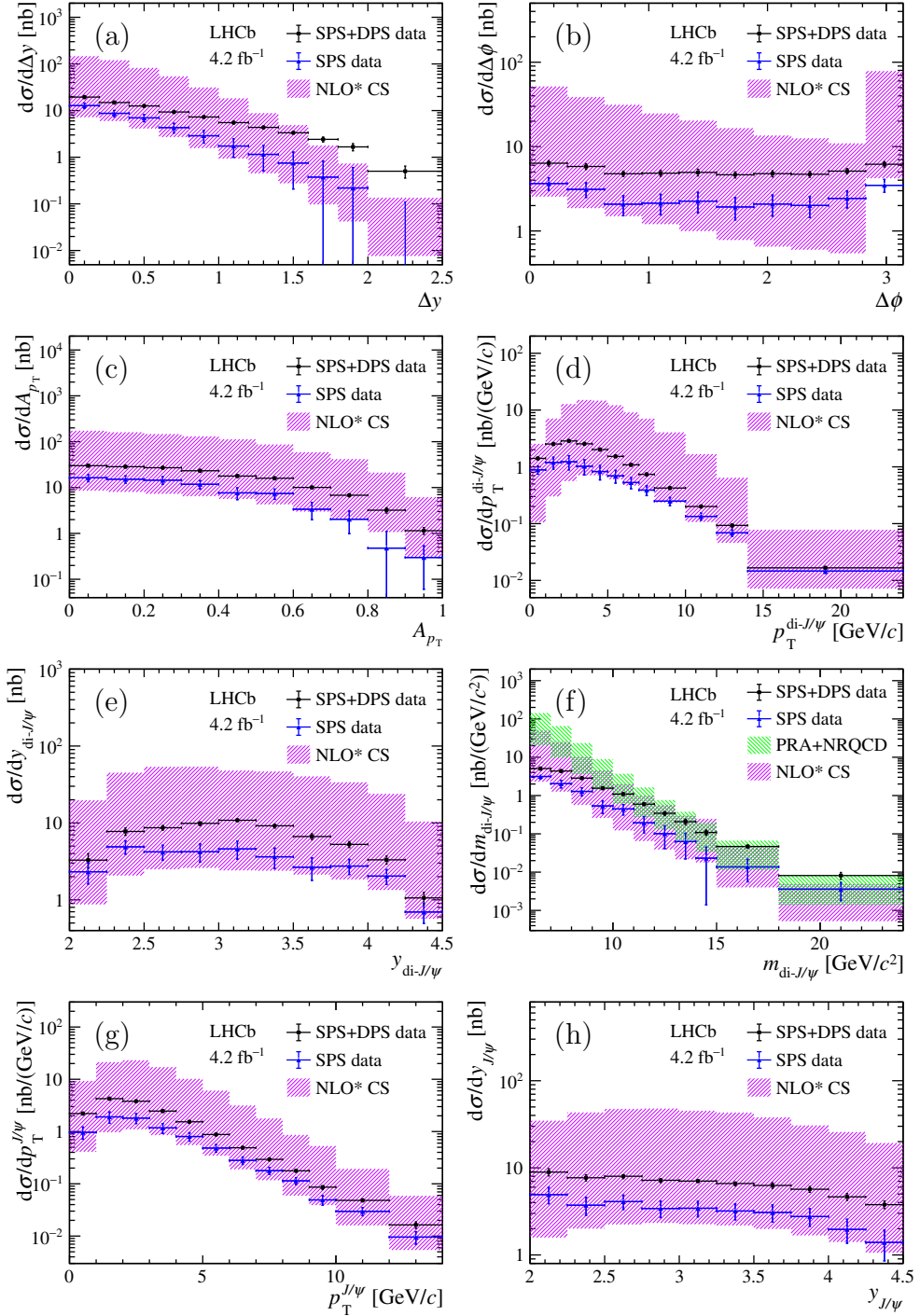


Figure 5: Differential cross-section of di- J/ψ production for SPS+DPS and SPS as a function of (a) Δy , (b) $\Delta\phi$, (c) A_{p_T} , (d) $p_T^{\text{di-}J/\psi}$, (e) $y_{\text{di-}J/\psi}$, (f) $m_{\text{di-}J/\psi}$, (g) $p_T^{J/\psi}$ and (h) $y_{J/\psi}$, compared with the NLO* CS predictions for SPS [74–76]. The $m_{\text{di-}J/\psi}$ spectrum is also compared with the PRA+NRQCD predictions for SPS [77].

sections are compared with the NLO* CS predictions, as shown in Fig. 5. The NLO* CS predictions include the uncertainties from the factorisation and renormalisation scales and subleading PDF uncertainties, correlated between the intervals. The measurements

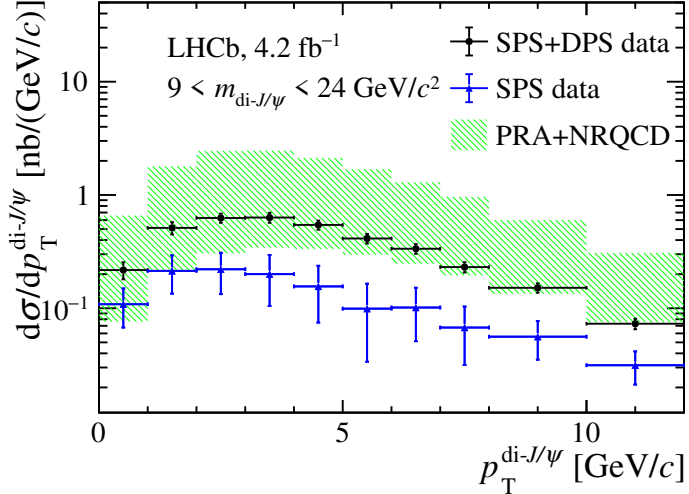


Figure 6: Differential cross-section of di- J/ψ production for SPS+DPS and SPS as a function of $p_T^{\text{di-}J/\psi}$ for candidates with $9 < m_{\text{di-}J/\psi} < 24 \text{ GeV}/c^2$, compared with the PRA+NRQCD predictions for SPS [77].

are consistent with the NLO* CS calculations within the large theoretical uncertainties. The mass spectrum is also compared with the predictions combining parton Reggeization approach (PRA) [78] and NRQCD factorisation [77], which includes a subset of higher-order QCD corrections without ad-hoc kinematic cuts. Only the renormalisation and factorisation scale uncertainties are considered in the predictions. In the large $m_{\text{di-}J/\psi}$ region, where the NRQCD-based calculations are well justified, there is a good agreement with the data, while the same predictions exceed the SPS data at small $m_{\text{di-}J/\psi}$, as shown in Fig. 5(f). The PRA+NRQCD calculations on the $p_T^{\text{di-}J/\psi}$ spectrum are thus further compared with that of the SPS data with $9 < m_{\text{di-}J/\psi} < 24 \text{ GeV}/c^2$, where the PRA+NRACD approach is expected to be validated, as shown in Fig. 6. The predictions are consistent with the SPS cross-sections at small $p_T^{\text{di-}J/\psi}$, but they overestimate the SPS data at $p_T^{\text{di-}J/\psi}$ larger than $3 \text{ GeV}/c$.

8 Study of gluon TMDs

The gluon TMD $h_1^{\perp g}(x, k_T^2, \mu)$ inside unpolarised protons, representing the distribution of linearly polarised gluons, can be probed through the distribution of the azimuthal angle ϕ_{CS} of either J/ψ meson in the Collins-Soper frame. This frame is the rest frame of the J/ψ pair with the polar axis (z -axis) bisecting the angle between the momentum of one proton and the reverse of the momentum of the other proton, the y -axis defined to be perpendicular to the plane spanned by the momenta of two protons, and the x -axis defined to complete a right-handed Cartesian coordinate system [79]. The prediction of the differential di- J/ψ production cross-section as a function of ϕ_{CS} through SPS is proportional to $a + b \times \cos(2\phi_{\text{CS}}) + c \times \cos(4\phi_{\text{CS}})$. The parameters a , b and c encode

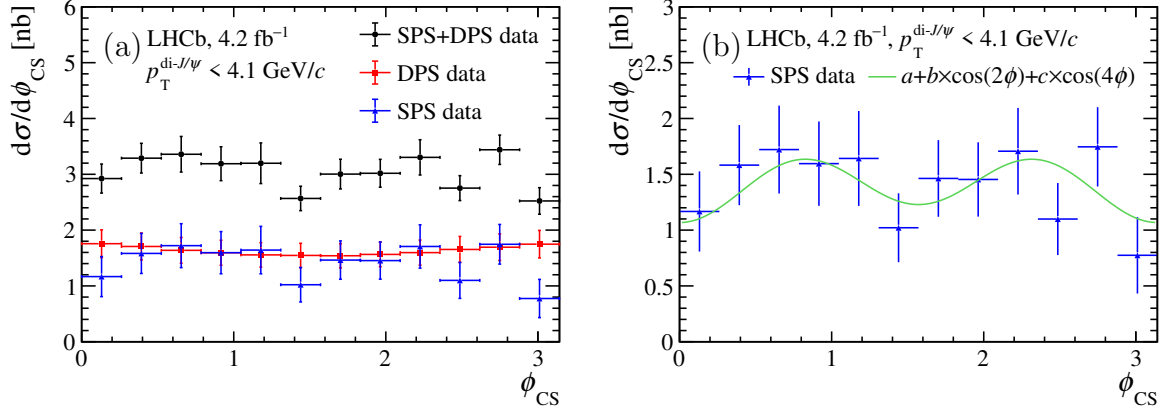


Figure 7: Distribution of ϕ_{CS} (a) with the SPS and DPS contributions separated in the TMD region $p_T^{\text{di}-J/\psi} < 4.1 \text{ GeV}/c$ and (b) for SPS with the function described in the text overlaid. The systematic uncertainties correlated between intervals are excluded from the error bars.

information on the gluon TMDs as

$$a = F_1 \mathcal{C}[f_1^g f_1^g] + F_2 \mathcal{C}[w_2 h_1^{\perp g} h_1^{\perp g}], \quad (10)$$

$$b = F_3 \mathcal{C}[w_3 f_1^g h_1^{\perp g}] + F'_3 \mathcal{C}[w'_3 h_1^{\perp g} f_1^g], \quad (11)$$

$$c = F_4 \mathcal{C}[w_4 h_1^{\perp g} h_1^{\perp g}], \quad (12)$$

where $F_i(')$ are hard-scattering coefficients, $w_i(')$ are the TMD weights common to all gluon-fusion processes originating from unpolarised proton collisions, and \mathcal{C} denotes the TMD convolutions [17, 18]. The calculation is valid in the TMD region with $p_T^{\text{di}-J/\psi} < \langle m_{\text{di}-J/\psi} \rangle / 2$ [17, 18]. In this analysis, the ϕ_{CS} distribution is measured in the TMD region $p_T^{\text{di}-J/\psi} < 4.1 \text{ GeV}/c$, since the average value of $m_{\text{di}-J/\psi}$ in the whole fiducial range is $\langle m_{\text{di}-J/\psi} \rangle = 8.2 \text{ GeV}/c^2$. The measured ϕ_{CS} distributions with the SPS and DPS contributions separated are shown in Fig. 7(a). The expectation values $\langle \cos 2\phi_{\text{CS}} \rangle$ and $\langle \cos 4\phi_{\text{CS}} \rangle$ correspond to half of the ratio of the $\cos n\phi_{\text{CS}}$ -modulations present in the TMD cross-section regarding its ϕ_{CS} -independent component [18], *i.e.* $\langle \cos 2\phi_{\text{CS}} \rangle = b/2a$ and $\langle \cos 4\phi_{\text{CS}} \rangle = c/2a$. They are calculated as

$$\langle \cos 2\phi_{\text{CS}} \rangle = \frac{\sum_i \frac{d\sigma}{d\phi_{\text{CS}}} |_i \Delta\phi_{\text{CS}i} \cos 2\phi_{\text{CS}i}}{\sum_i \frac{d\sigma}{d\phi_{\text{CS}}} |_i \Delta\phi_{\text{CS}i}}, \quad (13)$$

$$\langle \cos 4\phi_{\text{CS}} \rangle = \frac{\sum_i \frac{d\sigma}{d\phi_{\text{CS}}} |_i \Delta\phi_{\text{CS}i} \cos 4\phi_{\text{CS}i}}{\sum_i \frac{d\sigma}{d\phi_{\text{CS}}} |_i \Delta\phi_{\text{CS}i}}, \quad (14)$$

where the index i denotes each interval, $\Delta\phi_{\text{CS}i}$ is the interval width and $\phi_{\text{CS}i}$ is the interval centre. The results of $\langle \cos 2\phi_{\text{CS}} \rangle$ and $\langle \cos 4\phi_{\text{CS}} \rangle$ extracted from the ϕ_{CS} distribution for SPS are

$$\begin{aligned} \langle \cos 2\phi_{\text{CS}} \rangle &= -0.029 \pm 0.050 \text{ (stat)} \pm 0.009 \text{ (syst)}, \\ \langle \cos 4\phi_{\text{CS}} \rangle &= -0.087 \pm 0.052 \text{ (stat)} \pm 0.013 \text{ (syst)}, \end{aligned}$$

dominated by statistical uncertainties. The corresponding ϕ_{CS} function given by $a + b \times \cos(2\phi_{\text{CS}}) + c \times \cos(4\phi_{\text{CS}})$ is overlaid on the SPS result in Fig. 7(b). Its coefficients are

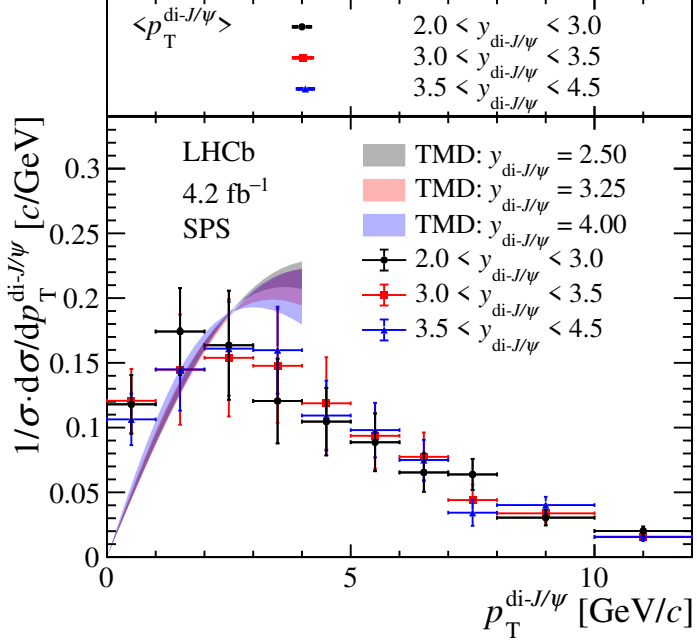


Figure 8: Normalised p_T spectrum of di- J/ψ production in different $y_{\text{di-}J/\psi}$ intervals, compared with TMD predictions [18] in the TMD region $p_T^{\text{di-}J/\psi} < \langle m_{\text{di-}J/\psi} \rangle / 2$. The average values of the $p_T^{\text{di-}J/\psi}$ distributions in three $y_{\text{di-}J/\psi}$ intervals are presented at the top of the figure.

fixed to the values calculated by Eqs. 13 and 14, and the normalisation is fixed to that of the SPS measurement. The results are consistent with zero, but the presence of an azimuthal asymmetry at a few percent level is allowed. The prediction of $\langle \cos 2\phi_{\text{CS}} \rangle$ varies from 0.009 to 0.016 due to nonperturbative uncertainties [18], also consistent with the measured result given the large uncertainty so far.

The p_T spectrum of the di- J/ψ signals from SPS can also be used to probe the gluon TMDs, especially $f_1^g(x, k_T^2, \mu)$ [17, 18]. It was pointed out in Ref. [18] that the variation of the momentum fractions of the two interacting gluons, $x_{1,2} = m_{\text{di-}J/\psi} e^{\pm y_{\text{di-}J/\psi}} / \sqrt{s}$, do not have significant impact on the shape of the $p_T^{\text{di-}J/\psi}$ spectrum. The $p_T^{\text{di-}J/\psi}$ spectrum is thus measured in three different intervals of $y_{\text{di-}J/\psi}$ for the SPS process, and the cross-section results are listed in Tables 18 and 19 in Appendix A for SPS+DPS and SPS separately. The distributions are normalised for comparison in Fig. 8. They are consistent with each other within the uncertainties. The average values of the $p_T^{\text{di-}J/\psi}$ distributions in three $y_{\text{di-}J/\psi}$ intervals are also presented at the top of Fig. 8, and show no significant variations. The TMD predictions [18], which are only applicable in the TMD region $p_T^{\text{di-}J/\psi} < \langle m_{\text{di-}J/\psi} \rangle / 2$, are also shown in Fig. 8, and peak at higher $p_T^{\text{di-}J/\psi}$ than the measured distributions.

In addition, the study of the dependence of TMDs on the renormalisation and rapidity scales, requires a measurement of the p_T spectrum at different $m_{\text{di-}J/\psi}$ [18]. The differential cross-sections $d\sigma/dp_T^{\text{di-}J/\psi}$ in the three intervals $6 < m_{\text{di-}J/\psi} < 7 \text{ GeV}/c^2$, $7 < m_{\text{di-}J/\psi} < 9 \text{ GeV}/c^2$ and $9 < m_{\text{di-}J/\psi} < 24 \text{ GeV}/c^2$, are listed in Tables 20 and 21 in Appendix A for SPS+DPS and SPS separately. The normalised p_T spectra of the di- J/ψ production for SPS in different $m_{\text{di-}J/\psi}$ intervals with the expected values of $\langle m_{\text{di-}J/\psi} \rangle = 6.6$, 7.9 and $11.0 \text{ GeV}/c^2$, respectively, are compared in Figure 9, with the TMD predictions [18]

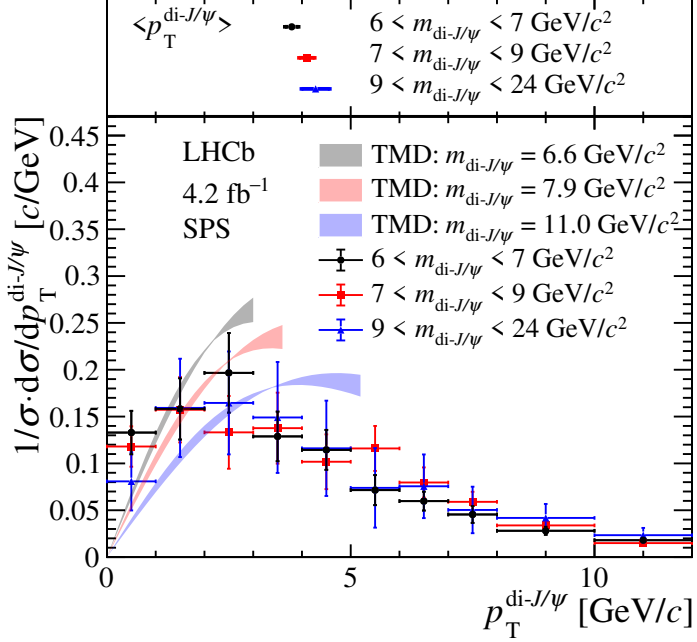


Figure 9: Normalised p_T spectrum of di- J/ψ production in three $m_{\text{di-}J/\psi}$ intervals with $\langle m_{\text{di-}J/\psi} \rangle = 6.6, 7.9$ and $11.0 \text{ GeV}/c^2$, compared with TMD predictions [18] in the TMD region $p_T^{\text{di-}J/\psi} < \langle m_{\text{di-}J/\psi} \rangle/2$. The average values of the $p_T^{\text{di-}J/\psi}$ distributions in three $m_{\text{di-}J/\psi}$ intervals are presented at the top of the figure.

overlaid in the TMD region. According to the prediction, the p_T spectrum would broaden as $m_{\text{di-}J/\psi}$ increases [18], but no obvious broadening of the p_T spectrum can be seen in the TMD region due to the large uncertainties. The average values of the $p_T^{\text{di-}J/\psi}$ distributions in three $m_{\text{di-}J/\psi}$ intervals are also presented at the top of Fig. 9, and slightly increase with mass.

9 Conclusion

The J/ψ -pair production cross-section in pp collisions at $\sqrt{s} = 13 \text{ TeV}$ is measured to be $16.36 \pm 0.28 \text{ (stat)} \pm 0.88 \text{ (syst)} \text{ nb}$ using a data sample corresponding to an integrated luminosity of 4.2 fb^{-1} collected by the LHCb experiment, with both J/ψ mesons in the range of $p_T < 14 \text{ GeV}/c$ and $2.0 < y < 4.5$. The contributions from DPS and SPS are separated based on distinctive Δy dependences of their corresponding cross-sections. The effective cross-section characterising the DPS process is determined to be $\sigma_{\text{eff}} = 13.1 \pm 1.8 \text{ (stat)} \pm 2.3 \text{ (syst)} \text{ mb}$, and is consistent with most of the existing measurements. The differential cross-sections in SPS are consistent with the NLO* CS predictions which are plagued by large theoretical uncertainties. The cross-sections predicted by PRA+NRQCD overshoot the SPS data at small $m_{\text{di-}J/\psi}$ and agree with them at large $m_{\text{di-}J/\psi}$.

The gluon TMDs are probed via the ϕ_{CS} distribution and the $p_T^{\text{di-}J/\psi}$ spectrum from the SPS process. The extracted values of $\langle \cos 2\phi_{\text{CS}} \rangle$ and $\langle \cos 4\phi_{\text{CS}} \rangle$ are consistent with zero, but the presence of an azimuthal asymmetry at a few percent level is allowed. The

$p_T^{\text{di-}J/\psi}$ spectra are consistent with each other in different $y_{\text{di-}J/\psi}$ intervals, and peak at lower $p_T^{\text{di-}J/\psi}$ values than the theoretical predictions. No significant broadening of the p_T spectrum with increasing $m_{\text{di-}J/\psi}$ is seen in the TMD region, but the average value of the $p_T^{\text{di-}J/\psi}$ distribution increases slightly with $m_{\text{di-}J/\psi}$. The results provide important experimental inputs to study gluon TMDs and to improve theoretical models. The ongoing data taking by the LHCb experiment will enable more precise measurements of production cross-sections, and allow to test the predictions of gluon TMDs with higher precision.

Acknowledgements

We would like to thank J.-P. Lansberg, H.-S. Shao, Y.-Q. Ma and L.-P. Sun for the helpful discussions on the quarkonium and quarkonium-pair production, and J.-P. Lansberg, H.-S. Shao, D. Boer, J. Bor, A. Colpani Serri, Z.-G. He and M. A. Nefedov for providing the SPS calculations. We express our gratitude to our colleagues in the CERN accelerator departments for the excellent performance of the LHC. We thank the technical and administrative staff at the LHCb institutes. We acknowledge support from CERN and from the national agencies: CAPES, CNPq, FAPERJ and FINEP (Brazil); MOST and NSFC (China); CNRS/IN2P3 (France); BMBF, DFG and MPG (Germany); INFN (Italy); NWO (Netherlands); MNiSW and NCN (Poland); MCID/IFA (Romania); MICINN (Spain); SNSF and SER (Switzerland); NASU (Ukraine); STFC (United Kingdom); DOE NP and NSF (USA). We acknowledge the computing resources that are provided by CERN, IN2P3 (France), KIT and DESY (Germany), INFN (Italy), SURF (Netherlands), PIC (Spain), GridPP (United Kingdom), CSCS (Switzerland), IFIN-HH (Romania), CBPF (Brazil), and Polish WLCG (Poland). We are indebted to the communities behind the multiple open-source software packages on which we depend. Individual groups or members have received support from ARC and ARDC (Australia); Key Research Program of Frontier Sciences of CAS, CAS PIFI, CAS CCEPP, Fundamental Research Funds for the Central Universities, and Sci. & Tech. Program of Guangzhou (China); Minciencias (Colombia); EPLANET, Marie Skłodowska-Curie Actions, ERC and NextGenerationEU (European Union); A*MIDEX, ANR, IPhU and Labex P2IO, and Région Auvergne-Rhône-Alpes (France); AvH Foundation (Germany); ICSC (Italy); GVA, XuntaGal, GENCAT, Inditex, InTalent and Prog. Atracción Talento, CM (Spain); SRC (Sweden); the Leverhulme Trust, the Royal Society and UKRI (United Kingdom).

A Differential cross-sections

The measured differential cross-sections of di- J/ψ production as functions of Δy , $\Delta\phi$, \mathcal{A}_{p_T} , $p_T^{\text{di-}J/\psi}$, $y_{\text{di-}J/\psi}$, $m_{\text{di-}J/\psi}$, $p_T^{J/\psi}$ and $y_{J/\psi}$ are listed in Tables 2–9. The differential cross-sections of di- J/ψ production for SPS process are listed in Tables 10–17. The differential cross-sections $d\sigma/dp_T^{\text{di-}J/\psi}$ in three different intervals of $y_{\text{di-}J/\psi}$ are listed in Tables 18 and 19 for SPS+DPS and SPS separately. The differential cross-sections $d\sigma/dp_T^{\text{di-}J/\psi}$ in three intervals of $m_{\text{di-}J/\psi}$ are listed in Tables 20 and 21 for SPS+DPS and SPS separately.

Table 2: Differential cross-sections $d\sigma/d\Delta y$ of di- J/ψ production. The first uncertainties are statistical, and the second systematic.

Δy	$d\sigma/d\Delta y$ [nb]
0.0–0.2	$19.46 \pm 0.87 \pm 1.15$
0.2–0.4	$14.88 \pm 0.56 \pm 0.81$
0.4–0.6	$12.57 \pm 0.50 \pm 0.69$
0.6–0.8	$9.32 \pm 0.37 \pm 0.52$
0.8–1.0	$7.29 \pm 0.33 \pm 0.41$
1.0–1.2	$5.52 \pm 0.28 \pm 0.31$
1.2–1.4	$4.36 \pm 0.27 \pm 0.24$
1.4–1.6	$3.34 \pm 0.26 \pm 0.21$
1.6–1.8	$2.42 \pm 0.26 \pm 0.15$
1.8–2.0	$1.67 \pm 0.23 \pm 0.18$
2.0–2.5	$0.50 \pm 0.13 \pm 0.05$

Table 3: Differential cross-sections $d\sigma/d\Delta\phi$ of di- J/ψ production. The first uncertainties are statistical, and the second systematic.

$\Delta\phi/\pi$	$d\sigma/d\Delta\phi$ [nb]
0.0–0.1	$6.35 \pm 0.30 \pm 0.37$
0.1–0.2	$5.81 \pm 0.31 \pm 0.34$
0.2–0.3	$4.77 \pm 0.24 \pm 0.27$
0.3–0.4	$4.84 \pm 0.30 \pm 0.27$
0.4–0.5	$4.95 \pm 0.35 \pm 0.29$
0.5–0.6	$4.64 \pm 0.27 \pm 0.27$
0.6–0.7	$4.78 \pm 0.30 \pm 0.27$
0.7–0.8	$4.70 \pm 0.25 \pm 0.27$
0.8–0.9	$5.12 \pm 0.23 \pm 0.29$
0.9–1.0	$6.18 \pm 0.29 \pm 0.35$

Table 4: Differential cross-sections $d\sigma/dA_{p_T}$ of di- J/ψ production. The first uncertainties are statistical, and the second systematic.

A_{p_T}	$d\sigma/dA_{p_T}$ [nb]
0.0–0.1	$29.98 \pm 1.17 \pm 1.68$
0.1–0.2	$28.50 \pm 1.04 \pm 1.59$
0.2–0.3	$27.06 \pm 1.34 \pm 1.52$
0.3–0.4	$23.23 \pm 1.06 \pm 1.30$
0.4–0.5	$17.82 \pm 1.04 \pm 1.10$
0.5–0.6	$15.95 \pm 0.80 \pm 0.98$
0.6–0.7	$10.06 \pm 0.64 \pm 0.56$
0.7–0.8	$6.79 \pm 0.59 \pm 0.37$
0.8–0.9	$3.21 \pm 0.38 \pm 0.21$
0.9–1.0	$1.14 \pm 0.18 \pm 0.08$

Table 5: Differential cross-sections $d\sigma/dp_T^{\text{di-}J/\psi}$ of di- J/ψ production. The first uncertainties are statistical, and the second systematic.

$p_T^{\text{di-}J/\psi}$ [GeV/ c]	$d\sigma/dp_T^{\text{di-}J/\psi}$ [nb/(GeV/ c)]
0–1	$1.408 \pm 0.089 \pm 0.083$
1–2	$2.523 \pm 0.126 \pm 0.150$
2–3	$2.858 \pm 0.158 \pm 0.164$
3–4	$2.542 \pm 0.110 \pm 0.146$
4–5	$2.017 \pm 0.081 \pm 0.120$
5–6	$1.527 \pm 0.073 \pm 0.091$
6–7	$1.085 \pm 0.048 \pm 0.065$
7–8	$0.738 \pm 0.038 \pm 0.044$
8–10	$0.424 \pm 0.018 \pm 0.027$
10–12	$0.200 \pm 0.011 \pm 0.013$
12–14	$0.093 \pm 0.007 \pm 0.005$
14–24	$0.017 \pm 0.001 \pm 0.001$

Table 6: Differential cross-sections $d\sigma/dy_{\text{di-}J/\psi}$ of di- J/ψ production. The first uncertainties are statistical, and the second systematic.

$y_{\text{di-}J/\psi}$	$d\sigma/dy_{\text{di-}J/\psi}$ [nb]
2.00–2.25	$3.28 \pm 0.64 \pm 0.29$
2.25–2.50	$7.75 \pm 0.53 \pm 0.69$
2.50–2.75	$8.66 \pm 0.36 \pm 0.52$
2.75–3.00	$9.88 \pm 0.32 \pm 0.59$
3.00–3.25	$10.83 \pm 0.32 \pm 0.62$
3.25–3.50	$9.18 \pm 0.30 \pm 0.54$
3.50–3.75	$6.66 \pm 0.21 \pm 0.54$
3.75–4.00	$5.26 \pm 0.19 \pm 0.44$
4.00–4.25	$3.31 \pm 0.19 \pm 0.35$
4.25–4.50	$1.06 \pm 0.16 \pm 0.12$

Table 7: Differential cross-sections $d\sigma/dm_{\text{di-}J/\psi}$ of di- J/ψ production. The first uncertainties are statistical, and the second systematic.

$m_{\text{di-}J/\psi}$ [GeV/ c]	$d\sigma/dm_{\text{di-}J/\psi}$ [nb/(GeV/ c)]
6–7	$5.059 \pm 0.200 \pm 0.283$
7–8	$4.364 \pm 0.131 \pm 0.244$
8–9	$2.851 \pm 0.092 \pm 0.155$
9–10	$1.555 \pm 0.067 \pm 0.085$
10–11	$1.092 \pm 0.062 \pm 0.062$
11–12	$0.595 \pm 0.049 \pm 0.034$
12–13	$0.344 \pm 0.037 \pm 0.026$
13–14	$0.207 \pm 0.029 \pm 0.016$
14–15	$0.108 \pm 0.015 \pm 0.008$
15–18	$0.047 \pm 0.005 \pm 0.003$
18–24	$0.008 \pm 0.002 \pm 0.001$

Table 8: Differential cross-sections $d\sigma/dp_T^{J/\psi}$ of di- J/ψ production. The first uncertainties are statistical, and the second systematic.

$p_T^{J/\psi}$ [GeV/ c]	$d\sigma/dp_T^{J/\psi}$ [nb/(GeV/ c)]
0–1	$2.209 \pm 0.093 \pm 0.132$
1–2	$4.255 \pm 0.124 \pm 0.255$
2–3	$3.798 \pm 0.090 \pm 0.208$
3–4	$2.464 \pm 0.062 \pm 0.135$
4–5	$1.536 \pm 0.044 \pm 0.085$
5–6	$0.878 \pm 0.027 \pm 0.048$
6–7	$0.489 \pm 0.019 \pm 0.028$
7–8	$0.293 \pm 0.013 \pm 0.016$
8–9	$0.177 \pm 0.010 \pm 0.011$
9–10	$0.086 \pm 0.007 \pm 0.005$
10–12	$0.048 \pm 0.003 \pm 0.003$
12–14	$0.016 \pm 0.002 \pm 0.001$

Table 9: Differential cross-sections $d\sigma/dy_{J/\psi}$ of di- J/ψ production. The first uncertainties are statistical, and the second systematic.

$y_{J/\psi}$	$d\sigma/dy_{J/\psi}$ [nb]
2.00–2.25	$8.93 \pm 0.56 \pm 0.65$
2.25–2.50	$7.69 \pm 0.29 \pm 0.56$
2.50–2.75	$8.01 \pm 0.21 \pm 0.44$
2.75–3.00	$7.20 \pm 0.18 \pm 0.39$
3.00–3.25	$7.05 \pm 0.16 \pm 0.38$
3.25–3.50	$6.61 \pm 0.15 \pm 0.36$
3.50–3.75	$6.28 \pm 0.15 \pm 0.45$
3.75–4.00	$5.68 \pm 0.15 \pm 0.41$
4.00–4.25	$4.65 \pm 0.16 \pm 0.39$
4.25–4.50	$3.78 \pm 0.20 \pm 0.32$

Table 10: Differential cross-sections $d\sigma/d\Delta y$ of di- J/ψ production in SPS. The first uncertainties are statistical, and the second systematic.

Δy	$d\sigma/d\Delta y$ [nb]
0.0–0.2	$12.76 \pm 1.29 \pm 1.13$
0.2–0.4	$8.72 \pm 1.03 \pm 0.85$
0.4–0.6	$6.97 \pm 0.94 \pm 0.74$
0.6–0.8	$4.32 \pm 0.80 \pm 0.62$
0.8–1.0	$2.89 \pm 0.70 \pm 0.53$
1.0–1.2	$1.74 \pm 0.60 \pm 0.43$
1.2–1.4	$1.15 \pm 0.53 \pm 0.37$
1.4–1.6	$0.75 \pm 0.45 \pm 0.31$
1.6–1.8	$0.37 \pm 0.39 \pm 0.24$
1.8–2.0	$0.22 \pm 0.31 \pm 0.22$
2.0–2.5	$-0.07 \pm 0.16 \pm 0.08$

Table 11: Differential cross-sections $d\sigma/d\Delta\phi$ of di- J/ψ production in SPS. The first uncertainties are statistical, and the second systematic.

$\Delta\phi/\pi$	$d\sigma/d\Delta\phi$ [nb]
0.0–0.1	$3.65 \pm 0.48 \pm 0.39$
0.1–0.2	$3.11 \pm 0.49 \pm 0.37$
0.2–0.3	$2.08 \pm 0.45 \pm 0.33$
0.3–0.4	$2.14 \pm 0.48 \pm 0.33$
0.4–0.5	$2.26 \pm 0.52 \pm 0.34$
0.5–0.6	$1.93 \pm 0.47 \pm 0.33$
0.6–0.7	$2.09 \pm 0.48 \pm 0.33$
0.7–0.8	$2.01 \pm 0.46 \pm 0.33$
0.8–0.9	$2.43 \pm 0.44 \pm 0.34$
0.9–1.0	$3.48 \pm 0.48 \pm 0.37$

Table 12: Differential cross-sections $d\sigma/d\mathcal{A}_{p_T}$ of di- J/ψ production in SPS. The first uncertainties are statistical, and the second systematic.

\mathcal{A}_{p_T}	$d\sigma/d\mathcal{A}_{p_T}$ [nb]
0.0–0.1	$16.31 \pm 2.26 \pm 1.83$
0.1–0.2	$15.19 \pm 2.15 \pm 1.76$
0.2–0.3	$14.50 \pm 2.22 \pm 1.67$
0.3–0.4	$11.78 \pm 1.93 \pm 1.48$
0.4–0.5	$7.65 \pm 1.77 \pm 1.32$
0.5–0.6	$7.41 \pm 1.44 \pm 1.14$
0.6–0.7	$3.37 \pm 1.14 \pm 0.77$
0.7–0.8	$2.04 \pm 0.90 \pm 0.54$
0.8–0.9	$0.48 \pm 0.54 \pm 0.32$
0.9–1.0	$0.30 \pm 0.21 \pm 0.10$

Table 13: Differential cross-sections $d\sigma/dp_T^{\text{di-}J/\psi}$ of di- J/ψ production in SPS. The first uncertainties are statistical, and the second systematic.

$p_T^{\text{di-}J/\psi}$ [GeV/ c]	$d\sigma/dp_T^{\text{di-}J/\psi}$ [nb/(GeV/ c)]
0–1	$0.886 \pm 0.116 \pm 0.084$
1–2	$1.196 \pm 0.225 \pm 0.173$
2–3	$1.229 \pm 0.279 \pm 0.201$
3–4	$1.026 \pm 0.241 \pm 0.184$
4–5	$0.827 \pm 0.186 \pm 0.149$
5–6	$0.693 \pm 0.139 \pm 0.107$
6–7	$0.529 \pm 0.092 \pm 0.074$
7–8	$0.390 \pm 0.062 \pm 0.048$
8–10	$0.249 \pm 0.031 \pm 0.028$
10–12	$0.134 \pm 0.014 \pm 0.013$
12–14	$0.069 \pm 0.008 \pm 0.005$
14–24	$0.015 \pm 0.001 \pm 0.001$

Table 14: Differential cross-sections $d\sigma/dy_{\text{di-}J/\psi}$ of di- J/ψ production in SPS. The first uncertainties are statistical, and the second systematic.

$y_{\text{di-}J/\psi}$	$d\sigma/dy_{\text{di-}J/\psi}$ [nb]
2.00–2.25	$2.32 \pm 0.65 \pm 0.29$
2.25–2.50	$4.89 \pm 0.67 \pm 0.69$
2.50–2.75	$4.20 \pm 0.72 \pm 0.59$
2.75–3.00	$4.21 \pm 0.86 \pm 0.72$
3.00–3.25	$4.59 \pm 0.94 \pm 0.77$
3.25–3.50	$3.63 \pm 0.84 \pm 0.68$
3.50–3.75	$2.66 \pm 0.60 \pm 0.62$
3.75–4.00	$2.75 \pm 0.40 \pm 0.46$
4.00–4.25	$2.04 \pm 0.26 \pm 0.36$
4.25–4.50	$0.70 \pm 0.16 \pm 0.12$

Table 15: Differential cross-sections $d\sigma/dm_{\text{di-}J/\psi}$ of di- J/ψ production in SPS. The first uncertainties are statistical, and the second systematic.

$m_{\text{di-}J/\psi}$ [GeV/ c]	$d\sigma/dm_{\text{di-}J/\psi}$ [nb/(GeV/ c)]
6–7	$3.147 \pm 0.336 \pm 0.286$
7–8	$2.039 \pm 0.353 \pm 0.290$
8–9	$1.283 \pm 0.240 \pm 0.190$
9–10	$0.535 \pm 0.159 \pm 0.117$
10–11	$0.446 \pm 0.110 \pm 0.078$
11–12	$0.194 \pm 0.075 \pm 0.047$
12–13	$0.101 \pm 0.050 \pm 0.033$
13–14	$0.063 \pm 0.035 \pm 0.020$
14–15	$0.023 \pm 0.019 \pm 0.011$
15–18	$0.014 \pm 0.007 \pm 0.004$
18–24	$0.004 \pm 0.002 \pm 0.001$

Table 16: Differential cross-sections $d\sigma/dp_T^{J/\psi}$ of di- J/ψ production in SPS. The first uncertainties are statistical, and the second systematic.

$p_T^{J/\psi}$ [GeV/c]	$d\sigma/dp_T^{J/\psi}$ [nb/(GeV/c)]
0–1	$0.966 \pm 0.198 \pm 0.159$
1–2	$1.907 \pm 0.354 \pm 0.303$
2–3	$1.807 \pm 0.295 \pm 0.246$
3–4	$1.173 \pm 0.192 \pm 0.160$
4–5	$0.804 \pm 0.112 \pm 0.095$
5–6	$0.484 \pm 0.062 \pm 0.052$
6–7	$0.280 \pm 0.035 \pm 0.029$
7–8	$0.178 \pm 0.021 \pm 0.017$
8–9	$0.114 \pm 0.014 \pm 0.011$
9–10	$0.049 \pm 0.009 \pm 0.006$
10–12	$0.030 \pm 0.004 \pm 0.003$
12–14	$0.010 \pm 0.002 \pm 0.001$

Table 17: Differential cross-sections $d\sigma/dy_{J/\psi}$ of di- J/ψ production in SPS. The first uncertainties are statistical, and the second systematic.

$y_{J/\psi}$	$d\sigma/dy_{J/\psi}$ [nb]
2.00–2.25	$4.92 \pm 0.79 \pm 0.68$
2.25–2.50	$3.72 \pm 0.63 \pm 0.61$
2.50–2.75	$4.09 \pm 0.59 \pm 0.50$
2.75–3.00	$3.42 \pm 0.56 \pm 0.47$
3.00–3.25	$3.44 \pm 0.53 \pm 0.44$
3.25–3.50	$3.19 \pm 0.51 \pm 0.43$
3.50–3.75	$3.08 \pm 0.48 \pm 0.49$
3.75–4.00	$2.76 \pm 0.44 \pm 0.45$
4.00–4.25	$1.97 \pm 0.41 \pm 0.44$
4.25–4.50	$1.39 \pm 0.39 \pm 0.37$

Table 18: Differential cross-sections $d\sigma/dp_T^{\text{di-}J/\psi}$ [nb/(GeV/c)] of di- J/ψ production in intervals of $y_{\text{di-}J/\psi}$. The first uncertainties are statistical, and the second systematic.

$p_T^{\text{di-}J/\psi}$ [GeV/c]	$2.0 < y_{\text{di-}J/\psi} < 3.0$	$3.0 < y_{\text{di-}J/\psi} < 3.5$	$3.5 < y_{\text{di-}J/\psi} < 4.5$
0–1	$0.626 \pm 0.072 \pm 0.037$	$0.426 \pm 0.035 \pm 0.025$	$0.334 \pm 0.029 \pm 0.020$
1–2	$1.140 \pm 0.103 \pm 0.068$	$0.763 \pm 0.055 \pm 0.045$	$0.611 \pm 0.037 \pm 0.036$
2–3	$1.237 \pm 0.137 \pm 0.071$	$0.881 \pm 0.046 \pm 0.050$	$0.707 \pm 0.040 \pm 0.040$
3–4	$1.054 \pm 0.084 \pm 0.060$	$0.823 \pm 0.051 \pm 0.047$	$0.665 \pm 0.038 \pm 0.038$
4–5	$0.874 \pm 0.063 \pm 0.052$	$0.648 \pm 0.038 \pm 0.039$	$0.486 \pm 0.030 \pm 0.029$
5–6	$0.679 \pm 0.060 \pm 0.040$	$0.469 \pm 0.027 \pm 0.028$	$0.375 \pm 0.026 \pm 0.022$
6–7	$0.483 \pm 0.036 \pm 0.029$	$0.339 \pm 0.021 \pm 0.020$	$0.263 \pm 0.020 \pm 0.016$
7–8	$0.390 \pm 0.031 \pm 0.023$	$0.201 \pm 0.014 \pm 0.012$	$0.139 \pm 0.014 \pm 0.008$
8–10	$0.192 \pm 0.014 \pm 0.012$	$0.123 \pm 0.007 \pm 0.008$	$0.112 \pm 0.008 \pm 0.007$
10–12	$0.105 \pm 0.009 \pm 0.007$	$0.052 \pm 0.004 \pm 0.003$	$0.042 \pm 0.005 \pm 0.003$

Table 19: Differential cross-sections $d\sigma/dp_T^{\text{di-}J/\psi}$ [nb/(GeV/c)] of di- J/ψ production in SPS in intervals of $y_{\text{di-}J/\psi}$. The first uncertainties are statistical, and the second systematic.

$p_T^{\text{di-}J/\psi}$ [GeV/c]	$2.0 < y_{\text{di-}J/\psi} < 3.0$	$3.0 < y_{\text{di-}J/\psi} < 3.5$	$3.5 < y_{\text{di-}J/\psi} < 4.5$
0–1	$0.428 \pm 0.078 \pm 0.036$	$0.238 \pm 0.044 \pm 0.027$	$0.198 \pm 0.035 \pm 0.021$
1–2	$0.632 \pm 0.125 \pm 0.072$	$0.286 \pm 0.087 \pm 0.058$	$0.270 \pm 0.061 \pm 0.043$
2–3	$0.593 \pm 0.164 \pm 0.082$	$0.304 \pm 0.093 \pm 0.068$	$0.299 \pm 0.070 \pm 0.050$
3–4	$0.437 \pm 0.121 \pm 0.075$	$0.291 \pm 0.091 \pm 0.063$	$0.297 \pm 0.064 \pm 0.046$
4–5	$0.379 \pm 0.094 \pm 0.063$	$0.234 \pm 0.069 \pm 0.050$	$0.203 \pm 0.050 \pm 0.036$
5–6	$0.322 \pm 0.078 \pm 0.047$	$0.185 \pm 0.048 \pm 0.035$	$0.182 \pm 0.038 \pm 0.025$
6–7	$0.237 \pm 0.050 \pm 0.033$	$0.153 \pm 0.034 \pm 0.024$	$0.139 \pm 0.027 \pm 0.017$
7–8	$0.231 \pm 0.038 \pm 0.024$	$0.087 \pm 0.022 \pm 0.014$	$0.064 \pm 0.017 \pm 0.010$
8–10	$0.110 \pm 0.018 \pm 0.013$	$0.067 \pm 0.011 \pm 0.009$	$0.075 \pm 0.010 \pm 0.007$
10–12	$0.073 \pm 0.010 \pm 0.007$	$0.031 \pm 0.005 \pm 0.003$	$0.029 \pm 0.005 \pm 0.003$

Table 20: Differential cross-sections $d\sigma/dp_T^{\text{di-}J/\psi}$ [nb/(GeV/c)] of di- J/ψ production in intervals of $m_{\text{di-}J/\psi}$ [GeV/ c^2]. The first uncertainties are statistical, and the second systematic.

$p_T^{\text{di-}J/\psi}$ [GeV/c]	$6 < m_{\text{di-}J/\psi} < 7 \text{ GeV}/c^2$	$7 < m_{\text{di-}J/\psi} < 9 \text{ GeV}/c^2$	$9 < m_{\text{di-}J/\psi} < 24 \text{ GeV}/c^2$
0–1	$0.563 \pm 0.063 \pm 0.033$	$0.626 \pm 0.053 \pm 0.037$	$0.217 \pm 0.035 \pm 0.013$
1–2	$0.867 \pm 0.087 \pm 0.051$	$1.138 \pm 0.071 \pm 0.067$	$0.512 \pm 0.056 \pm 0.030$
2–3	$1.025 \pm 0.132 \pm 0.059$	$1.213 \pm 0.069 \pm 0.069$	$0.627 \pm 0.046 \pm 0.036$
3–4	$0.743 \pm 0.062 \pm 0.043$	$1.167 \pm 0.074 \pm 0.067$	$0.632 \pm 0.053 \pm 0.036$
4–5	$0.587 \pm 0.051 \pm 0.035$	$0.883 \pm 0.050 \pm 0.053$	$0.544 \pm 0.039 \pm 0.032$
5–6	$0.363 \pm 0.041 \pm 0.022$	$0.742 \pm 0.050 \pm 0.044$	$0.413 \pm 0.032 \pm 0.025$
6–7	$0.264 \pm 0.024 \pm 0.016$	$0.491 \pm 0.032 \pm 0.029$	$0.335 \pm 0.026 \pm 0.020$
7–8	$0.182 \pm 0.024 \pm 0.011$	$0.327 \pm 0.022 \pm 0.019$	$0.231 \pm 0.020 \pm 0.014$
8–10	$0.102 \pm 0.010 \pm 0.007$	$0.170 \pm 0.011 \pm 0.011$	$0.152 \pm 0.010 \pm 0.010$
10–12	$0.059 \pm 0.007 \pm 0.004$	$0.067 \pm 0.006 \pm 0.004$	$0.073 \pm 0.006 \pm 0.005$

Table 21: Differential cross-sections $d\sigma/dp_T^{\text{di-}J/\psi}$ [nb/(GeV/c)] of di- J/ψ production in SPS in intervals of $m_{\text{di-}J/\psi}$ [GeV/ c^2]. The first uncertainties are statistical, and the second systematic.

$p_T^{\text{di-}J/\psi}$ [GeV/c]	$6 < m_{\text{di-}J/\psi} < 7 \text{ GeV}/c^2$	$7 < m_{\text{di-}J/\psi} < 9 \text{ GeV}/c^2$	$9 < m_{\text{di-}J/\psi} < 24 \text{ GeV}/c^2$
0–1	$0.400 \pm 0.067 \pm 0.032$	$0.376 \pm 0.064 \pm 0.038$	$0.109 \pm 0.038 \pm 0.015$
1–2	$0.475 \pm 0.103 \pm 0.055$	$0.501 \pm 0.114 \pm 0.081$	$0.214 \pm 0.070 \pm 0.037$
2–3	$0.591 \pm 0.146 \pm 0.062$	$0.424 \pm 0.131 \pm 0.093$	$0.221 \pm 0.073 \pm 0.048$
3–4	$0.387 \pm 0.079 \pm 0.047$	$0.438 \pm 0.126 \pm 0.087$	$0.200 \pm 0.081 \pm 0.051$
4–5	$0.344 \pm 0.062 \pm 0.036$	$0.324 \pm 0.093 \pm 0.068$	$0.156 \pm 0.067 \pm 0.046$
5–6	$0.215 \pm 0.046 \pm 0.022$	$0.369 \pm 0.073 \pm 0.050$	$0.099 \pm 0.054 \pm 0.037$
6–7	$0.180 \pm 0.026 \pm 0.015$	$0.253 \pm 0.047 \pm 0.033$	$0.102 \pm 0.042 \pm 0.028$
7–8	$0.137 \pm 0.024 \pm 0.010$	$0.188 \pm 0.029 \pm 0.020$	$0.068 \pm 0.030 \pm 0.019$
8–10	$0.084 \pm 0.010 \pm 0.006$	$0.108 \pm 0.014 \pm 0.011$	$0.056 \pm 0.017 \pm 0.012$
10–12	$0.054 \pm 0.007 \pm 0.004$	$0.048 \pm 0.006 \pm 0.004$	$0.031 \pm 0.009 \pm 0.006$

References

- [1] CDF collaboration, T. Aaltonen *et al.*, *High-precision measurement of the W boson mass with the CDF II detector*, Science **376** (2022) 170.
- [2] D0 collaboration, V. M. Abazov *et al.*, *Measurement of the W boson mass with the D0 detector*, Phys. Rev. Lett. **108** (2012) 151804, [arXiv:1203.0293](https://arxiv.org/abs/1203.0293).
- [3] ATLAS collaboration, M. Aaboud *et al.*, *Measurement of the W-boson mass in pp collisions at $\sqrt{s} = 7$ TeV with the ATLAS detector*, Eur. Phys. J. **C78** (2018) 110, Erratum *ibid.* **C78** (2018) 898, [arXiv:1701.07240](https://arxiv.org/abs/1701.07240).
- [4] LHCb collaboration, R. Aaij *et al.*, *Measurement of the W boson mass*, JHEP **01** (2022) 036, [arXiv:2109.01113](https://arxiv.org/abs/2109.01113).
- [5] P. J. Mulders and J. Rodrigues, *Transverse momentum dependence in gluon distribution and fragmentation functions*, Phys. Rev. **D63** (2001) 094021, [arXiv:hep-ph/0009343](https://arxiv.org/abs/hep-ph/0009343).
- [6] F. Dominguez, C. Marquet, B.-W. Xiao, and F. Yuan, *Universality of unintegrated gluon distributions at small x*, Phys. Rev. **D83** (2011) 105005, [arXiv:1101.0715](https://arxiv.org/abs/1101.0715).
- [7] M. G. Echevarría, A. Idilbi, and I. Scimemi, *Soft and collinear factorization and transverse momentum dependent parton distribution functions*, Phys. Lett. **B726** (2013) 795, [arXiv:1211.1947](https://arxiv.org/abs/1211.1947).
- [8] HERMES collaboration, A. Airapetian *et al.*, *Observation of the naive-T-odd Sivers effect in deep-inelastic scattering*, Phys. Rev. Lett. **103** (2009) 152002, [arXiv:0906.3918](https://arxiv.org/abs/0906.3918).
- [9] COMPASS collaboration, G. D. Alexeev *et al.*, *Transverse-spin-dependent azimuthal asymmetries of pion and kaon pairs produced in muon-proton and muon-deuteron semi-inclusive deep inelastic scattering*, Phys. Lett. **B845** (2023) 138155, [arXiv:2301.02013](https://arxiv.org/abs/2301.02013).
- [10] NuSea collaboration, L. Y. Zhu *et al.*, *Measurement of angular distributions of Drell-Yan dimuons in p+d interaction at 800- GeV/c*, Phys. Rev. Lett. **99** (2007) 082301, [arXiv:hep-ex/0609005](https://arxiv.org/abs/hep-ex/0609005).
- [11] P. C. Barry *et al.*, *Tomography of pions and protons via transverse momentum dependent distributions*, [arXiv:2302.01192](https://arxiv.org/abs/2302.01192).
- [12] Jefferson Lab Hall A collaboration, Y. Zhang *et al.*, *Measurement of pretzelosity asymmetry of charged pion production in semi-inclusive deep inelastic scattering on a polarized ${}^3\text{He}$ target*, Phys. Rev. C **90** (2014) 055209, [arXiv:1312.3047](https://arxiv.org/abs/1312.3047).
- [13] CLAS collaboration, H. Avakian *et al.*, *Measurement of single and double spin asymmetries in deep inelastic pion electroproduction with a longitudinally polarized target*, Phys. Rev. Lett. **105** (2010) 262002, [arXiv:1003.4549](https://arxiv.org/abs/1003.4549).
- [14] D. Boer *et al.*, *Gluons and the quark sea at high energies: Distributions, polarization, tomography*, [arXiv:1108.1713](https://arxiv.org/abs/1108.1713).

- [15] LHCb collaboration, B. Passalacqua, P. Di Nezza, P. Lenisa, and L. L. Pappalardo, *The LHCspin project: A polarized fixed target for LHC*, Nuovo Cim. **C45** (2022) 121.
- [16] S. J. Brodsky, F. Fleuret, C. Hadjidakis, and J. P. Lansberg, *Physics opportunities of a fixed-target experiment using the LHC beams*, Phys. Rept. **522** (2013) 239, [arXiv:1202.6585](#).
- [17] J.-P. Lansberg, C. Pisano, F. Scarpa, and M. Schlegel, *Pinning down the linearly-polarised gluons inside unpolarised protons using quarkonium-pair production at the LHC*, Phys. Lett. **B784** (2018) 217, Erratum ibid. **B791** (2019) 420, [arXiv:1710.01684](#).
- [18] F. Scarpa *et al.*, *Studies of gluon TMDs and their evolution using quarkonium-pair production at the LHC*, Eur. Phys. J. **C80** (2020) 87, [arXiv:1909.05769](#).
- [19] LHCb collaboration, R. Aaij *et al.*, *Measurement of the J/ψ pair production cross-section in pp collisions at $\sqrt{s} = 13\text{ TeV}$* , JHEP **06** (2017) 047, Erratum ibid. **10** (2017) 068, [arXiv:1612.07451](#).
- [20] G. T. Bodwin, E. Braaten, and G. P. Lepage, *Rigorous QCD analysis of inclusive annihilation and production of heavy quarkonium*, Phys. Rev. **D51** (1995) 1125, Erratum ibid. **D55** (1997) 5853, [arXiv:hep-ph/9407339](#).
- [21] P. L. Cho and A. K. Leibovich, *Color octet quarkonia production*, Phys. Rev. **D53** (1996) 150, [arXiv:hep-ph/9505329](#).
- [22] P. L. Cho and A. K. Leibovich, *Color octet quarkonia production II*, Phys. Rev. **D53** (1996) 6203, [arXiv:hep-ph/9511315](#).
- [23] P. Zhang, C. Meng, Y.-Q. Ma, and K.-T. Chao, *Gluon fragmentation into ${}^3P_J^{[1,8]}$ quark pair and test of NRQCD factorization at two-loop level*, JHEP **08** (2021) 111, [arXiv:2011.04905](#).
- [24] L.-P. Sun, H. Han, and K.-T. Chao, *Impact of J/ψ pair production at the LHC and predictions in nonrelativistic QCD*, Phys. Rev. **D94** (2016) 074033, [arXiv:1404.4042](#).
- [25] J.-P. Lansberg, H.-S. Shao, N. Yamanaka, and Y.-J. Zhang, *Prompt J/ψ -pair production at the LHC: Impact of loop-induced contributions and of the colour-octet mechanism*, Eur. Phys. J. **C79** (2019) 1006, [arXiv:1906.10049](#).
- [26] A. K. Likhoded, A. V. Luchinsky, and S. V. Poslavsky, *Production of $J/\psi + \chi_c$ and $J/\psi + J/\psi$ with real gluon emission at LHC*, Phys. Rev. **D94** (2016) 054017, [arXiv:1606.06767](#).
- [27] S. P. Baranov, *Pair production of J/ψ mesons in the k_t -factorization approach*, Phys. Rev. **D84** (2011) 054012.
- [28] J.-P. Lansberg and H.-S. Shao, *J/ψ -pair production at large momenta: Indications for double parton scatterings and large α_s^5 contributions*, Phys. Lett. **B751** (2015) 479, [arXiv:1410.8822](#).

- [29] LHCb collaboration, R. Aaij *et al.*, *Associated production of prompt J/ψ and Υ mesons in pp collisions at $\sqrt{s} = 13$ TeV*, JHEP **08** (2023) 093, [arXiv:2305.15580](#).
- [30] ATLAS collaboration, G. Aad *et al.*, *Observation and measurements of the production of prompt and non-prompt J/ψ mesons in association with a Z boson in pp collisions at $\sqrt{s} = 8$ TeV with the ATLAS detector*, Eur. Phys. J. **C75** (2015) 229, [arXiv:1412.6428](#).
- [31] ATLAS collaboration, M. Aaboud *et al.*, *Measurement of the prompt J/ψ pair production cross-section in pp collisions at $\sqrt{s} = 8$ TeV with the ATLAS detector*, Eur. Phys. J. **C77** (2017) 76, [arXiv:1612.02950](#).
- [32] LHCb collaboration, R. Aaij *et al.*, *Production of associated Υ and open charm hadrons in pp collisions at $\sqrt{s} = 7$ and 8 TeV via double parton scattering*, JHEP **07** (2016) 052, [arXiv:1510.05949](#).
- [33] ATLAS collaboration, G. Aad *et al.*, *Measurement of the production cross section of prompt J/ψ mesons in association with a W^\pm boson in pp collisions at $\sqrt{s} = 7$ TeV with the ATLAS detector*, JHEP **04** (2014) 172, [arXiv:1401.2831](#).
- [34] CMS collaboration, V. Khachatryan *et al.*, *Measurement of prompt J/ψ pair production in pp collisions at $\sqrt{s} = 7$ TeV*, JHEP **09** (2014) 094, [arXiv:1406.0484](#).
- [35] LHCb collaboration, R. Aaij *et al.*, *Observation of double charm production involving open charm in pp collisions at $\sqrt{s} = 7$ TeV*, JHEP **06** (2012) 141, Addendum ibid. **03** (2014) 108, [arXiv:1205.0975](#).
- [36] ATLAS collaboration, G. Aad *et al.*, *Measurement of hard double-parton interactions in $W(\rightarrow l\nu) + 2$ -jet events at $\sqrt{s} = 7$ TeV with the ATLAS detector*, New J. Phys. **15** (2013) 033038, [arXiv:1301.6872](#).
- [37] CMS collaboration, S. Chatrchyan *et al.*, *Study of double parton scattering using $W + 2$ -jet events in proton-proton collisions at $\sqrt{s} = 7$ TeV*, JHEP **03** (2014) 032, [arXiv:1312.5729](#).
- [38] D0 collaboration, V. M. Abazov *et al.*, *Evidence for simultaneous production of J/ψ and Υ mesons*, Phys. Rev. Lett. **116** (2016) 082002, [arXiv:1511.02428](#).
- [39] D0 collaboration, V. M. Abazov *et al.*, *Observation and studies of double J/ψ production at the Tevatron*, Phys. Rev. **D90** (2014) 111101, [arXiv:1406.2380](#).
- [40] D0 collaboration, V. M. Abazov *et al.*, *Double parton interactions in $\gamma + 3$ -jet events in $p\bar{p}$ collisions $\sqrt{s} = 1.96$ TeV*, Phys. Rev. **D81** (2010) 052012, [arXiv:0912.5104](#).
- [41] CDF collaboration, F. Abe *et al.*, *Study of four jet events and evidence for double parton interactions in $p\bar{p}$ collisions at $\sqrt{s} = 1.8$ TeV*, Phys. Rev. **D47** (1993) 4857.
- [42] CDF collaboration, F. Abe *et al.*, *Double parton scattering in $\bar{p}p$ collisions at $\sqrt{s} = 1.8$ TeV*, Phys. Rev. **D56** (1997) 3811.
- [43] G. Calucci and D. Treleani, *Mini-jets and the two-body parton correlation*, Phys. Rev. **D57** (1998) 503, [arXiv:hep-ph/9707389](#).

- [44] G. Calucci and D. Treleani, *Proton structure in transverse space and the effective cross section*, Phys. Rev. **D60** (1999) 054023, [arXiv:hep-ph/9902479](#).
- [45] A. Del Fabbro and D. Treleani, *Scale factor in double parton collisions and parton densities in transverse space*, Phys. Rev. **D63** (2001) 057901, [arXiv:hep-ph/0005273](#).
- [46] LHCb collaboration, A. A. Alves Jr. *et al.*, *The LHCb detector at the LHC*, JINST **3** (2008) S08005.
- [47] LHCb collaboration, R. Aaij *et al.*, *LHCb detector performance*, Int. J. Mod. Phys. **A30** (2015) 1530022, [arXiv:1412.6352](#).
- [48] T. Sjöstrand, S. Mrenna, and P. Skands, *A brief introduction to PYTHIA 8.1*, Comput. Phys. Commun. **178** (2008) 852, [arXiv:0710.3820](#).
- [49] T. Sjöstrand, S. Mrenna, and P. Skands, *PYTHIA 6.4 physics and manual*, JHEP **05** (2006) 026, [arXiv:hep-ph/0603175](#).
- [50] I. Belyaev *et al.*, *Handling of the generation of primary events in Gauss, the LHCb simulation framework*, J. Phys. Conf. Ser. **331** (2011) 032047.
- [51] M. Bargiotti and V. Vagnoni, *Heavy quarkonia sector in PYTHIA 6.324: Tuning, validation and perspectives at LHC(b)*, CERN-LHCB-2007-042, 2007.
- [52] D. J. Lange, *The EvtGen particle decay simulation package*, Nucl. Instrum. Meth. **A462** (2001) 152.
- [53] N. Davidson, T. Przedzinski, and Z. Was, *PHOTOS interface in C++: Technical and physics documentation*, Comp. Phys. Comm. **199** (2016) 86, [arXiv:1011.0937](#).
- [54] Geant4 collaboration, J. Allison *et al.*, *Geant4 developments and applications*, IEEE Trans. Nucl. Sci. **53** (2006) 270.
- [55] Geant4 collaboration, S. Agostinelli *et al.*, *Geant4—A simulation toolkit*, Nucl. Instrum. Meth. **A506** (2003) 250.
- [56] M. Clemencic *et al.*, *The LHCb simulation application, Gauss: Design, evolution and experience*, J. Phys. Conf. Ser. **331** (2011) 032023.
- [57] R. Aaij *et al.*, *The LHCb trigger and its performance in 2011*, JINST **8** (2013) P04022, [arXiv:1211.3055](#).
- [58] Particle Data Group, R. L. Workman *et al.*, *Review of particle physics*, PTEP **2022** (2022) 083C01.
- [59] LHCb collaboration, R. Aaij *et al.*, *Measurement of J/ψ production in pp collisions at $\sqrt{s} = 7\text{ TeV}$* , Eur. Phys. J. **C71** (2011) 1645, [arXiv:1103.0423](#).
- [60] LHCb collaboration, R. Aaij *et al.*, *Precision luminosity measurements at LHCb*, JINST **9** (2014) P12005, [arXiv:1410.0149](#).

- [61] T. Skwarnicki, *A study of the radiative cascade transitions between the Upsilon-prime and Upsilon resonances*, PhD thesis, Institute of Nuclear Physics, Krakow, 1986, DESY-F31-86-02.
- [62] M. Pivk and F. R. Le Diberder, *sPlot: A statistical tool to unfold data distributions*, Nucl. Instrum. Meth. **A555** (2005) 356, [arXiv:physics/0402083](https://arxiv.org/abs/physics/0402083).
- [63] LHCb collaboration, R. Aaij *et al.*, *Measurement of the track reconstruction efficiency at LHCb*, JINST **10** (2015) P02007, [arXiv:1408.1251](https://arxiv.org/abs/1408.1251).
- [64] F. Archilli *et al.*, *Performance of the muon identification at LHCb*, JINST **8** (2013) P10020, [arXiv:1306.0249](https://arxiv.org/abs/1306.0249).
- [65] B. Efron, *Bootstrap methods: Another look at the Jackknife*, Annals Statist. **7** (1979) 1.
- [66] K. S. Cranmer, *Kernel estimation in high-energy physics*, Comput. Phys. Commun. **136** (2001) 198, [arXiv:hep-ex/0011057](https://arxiv.org/abs/hep-ex/0011057).
- [67] LHCb collaboration, R. Aaij *et al.*, *Measurement of J/ψ polarization in pp collisions at $\sqrt{s} = 7 \text{ TeV}$* , Eur. Phys. J. **C73** (2013) 2631, [arXiv:1307.6379](https://arxiv.org/abs/1307.6379).
- [68] LHCb collaboration, R. Aaij *et al.*, *Measurement of forward J/ψ production cross-sections in pp collisions at $\sqrt{s} = 13 \text{ TeV}$* , JHEP **10** (2015) 172, Erratum *ibid.* **05** (2017) 063, [arXiv:1509.00771](https://arxiv.org/abs/1509.00771).
- [69] C. H. Kom, A. Kulesza, and W. J. Stirling, *Pair production of J/ψ as a probe of double parton scattering at LHCb*, Phys. Rev. Lett. **107** (2011) 082002, [arXiv:1105.4186](https://arxiv.org/abs/1105.4186).
- [70] J.-P. Lansberg and H.-S. Shao, *Associated production of a quarkonium and a Z boson at one loop in a quark-hadron-duality approach*, JHEP **10** (2016) 153, [arXiv:1608.03198](https://arxiv.org/abs/1608.03198).
- [71] J.-P. Lansberg, H.-S. Shao, and N. Yamanaka, *Indication for double parton scatterings in $W +$ prompt J/ψ production at the LHC*, Phys. Lett. **B781** (2018) 485, [arXiv:1707.04350](https://arxiv.org/abs/1707.04350).
- [72] H.-S. Shao, *J/ψ meson production in association with an open charm hadron at the LHC: A reappraisal*, Phys. Rev. **D102** (2020) 034023, [arXiv:2005.12967](https://arxiv.org/abs/2005.12967).
- [73] H.-S. Shao and Y.-J. Zhang, *Complete study of hadroproduction of a Υ meson associated with a prompt J/ψ* , Phys. Rev. Lett. **117** (2016) 062001, [arXiv:1605.03061](https://arxiv.org/abs/1605.03061).
- [74] J.-P. Lansberg and H.-S. Shao, *Production of $J/\psi + \eta_c$ versus $J/\psi + J/\psi$ at the LHC: Importance of real α_s^5 corrections*, Phys. Rev. Lett. **111** (2013) 122001, [arXiv:1308.0474](https://arxiv.org/abs/1308.0474).
- [75] H.-S. Shao, *HELAC-Onia: An automatic matrix element generator for heavy quarkonium physics*, Comput. Phys. Commun. **184** (2013) 2562, [arXiv:1212.5293](https://arxiv.org/abs/1212.5293).
- [76] H.-S. Shao, *HELAC-Onia 2.0: An upgraded matrix-element and event generator for heavy quarkonium physics*, Comput. Phys. Commun. **198** (2016) 238, [arXiv:1507.03435](https://arxiv.org/abs/1507.03435).

- [77] Z.-G. He, B. A. Kniehl, M. A. Nefedov, and V. A. Saleev, *Double prompt J/ψ hadroproduction in the parton Reggeization approach with high-energy resummation*, Phys. Rev. Lett. **123** (2019) 162002, [arXiv:1906.08979](https://arxiv.org/abs/1906.08979).
- [78] A. V. Karpishkov, M. A. Nefedov, and V. A. Saleev, *$B\bar{B}$ angular correlations at the LHC in parton Reggeization approach merged with higher-order matrix elements*, Phys. Rev. **D96** (2017) 096019, [arXiv:1707.04068](https://arxiv.org/abs/1707.04068).
- [79] J. C. Collins and D. E. Soper, *Angular distribution of di-leptons in high-energy hadron collisions*, Phys. Rev. **D16** (1977) 2219.

V. Dedu¹² , L. Del Buono¹⁵ , B. Delaney⁶² , H.-P. Dembinski¹⁷ , J. Deng⁸ , V. Denysenko⁴⁸ , O. Deschamps¹¹ , F. Dettori^{29,i} , B. Dey⁷⁴ , P. Di Nezza²⁵ , I. Diachkov⁴¹ , S. Didenko⁴¹ , S. Ding⁶⁶ , V. Dobishuk⁵⁰ , A. D. Docheva⁵⁷ , A. Dolmatov⁴¹ , C. Dong⁴ , A.M. Donohoe²⁰ , F. Dordei²⁹ , A.C. dos Reis² , L. Douglas⁵⁷ , A.G. Downes¹⁰ , W. Duan⁶⁹ , P. Duda⁷⁷ , M.W. Dudek³⁸ , L. Dufour⁴⁶ , V. Duk³¹ , P. Durante⁴⁶ , M. M. Duras⁷⁷ , J.M. Durham⁶⁵ , D. Dutta⁶⁰ , A. Dziurda³⁸ , A. Dzyuba⁴¹ , S. Easo^{55,46} , E. Eckstein⁷³ , U. Egede¹ , A. Egorychev⁴¹ , V. Egorychev⁴¹ , C. Eirea Orro⁴⁴ , S. Eisenhardt⁵⁶ , E. Ejopu⁶⁰ , S. Ek-In⁴⁷ , L. Eklund⁷⁸ , M. Elashri⁶³ , J. Ellbracht¹⁷ , S. Ely⁵⁹ , A. Ene⁴⁰ , E. Epple⁶³ , S. Escher¹⁶ , J. Eschle⁴⁸ , S. Esen⁴⁸ , T. Evans⁶⁰ , F. Fabiano^{29,i,46} , L.N. Falcao² , Y. Fan⁷ , B. Fang^{71,13} , L. Fantini^{31,p} , M. Faria⁴⁷ , K. Farmer⁵⁶ , D. Fazzini^{28,n} , L. Felkowski⁷⁷ , M. Feng^{5,7} , M. Feo⁴⁶ , M. Fernandez Gomez⁴⁴ , A.D. Fernez⁶⁴ , F. Ferrari²² , F. Ferreira Rodrigues³ , S. Ferreres Sole³⁵ , M. Ferrillo⁴⁸ , M. Ferro-Luzzi⁴⁶ , S. Filippov⁴¹ , R.A. Fini²¹ , M. Fiorini^{23,j} , M. Firlej³⁷ , K.M. Fischer⁶¹ , D.S. Fitzgerald⁷⁹ , C. Fitzpatrick⁶⁰ , T. Fiutowski³⁷ , F. Fleuret¹⁴ , M. Fontana²² , F. Fontanelli^{26,l} , L. F. Foreman⁶⁰ , R. Forty⁴⁶ , D. Foulds-Holt⁵³ , M. Franco Sevilla⁶⁴ , M. Frank⁴⁶ , E. Franzoso^{23,j} , G. Frau¹⁹ , C. Frei⁴⁶ , D.A. Friday⁶⁰ , L. Frontini^{27,m} , J. Fu⁷ , Q. Fuehring¹⁷ , Y. Fujii¹ , T. Fulghesu¹⁵ , E. Gabriel³⁵ , G. Galati^{21,g} , M.D. Galati³⁵ , A. Gallas Torreira⁴⁴ , D. Galli^{22,h} , S. Gambetta^{56,46} , M. Gandelman³ , P. Gandini²⁷ , H. Gao⁷ , R. Gao⁶¹ , Y. Gao⁸ , Y. Gao⁶ , Y. Gao⁸ , M. Garau^{29,i} , L.M. Garcia Martin⁴⁷ , P. Garcia Moreno⁴³ , J. García Pardiñas⁴⁶ , B. Garcia Plana⁴⁴ , K. G. Garg⁸ , L. Garrido⁴³ , C. Gaspar⁴⁶ , R.E. Geertsema³⁵ , L.L. Gerken¹⁷ , E. Gersabeck⁶⁰ , M. Gersabeck⁶⁰ , T. Gershon⁵⁴ , Z. Ghorbanimoghaddam⁵² , L. Giambastiani³⁰ , F. I. Giasemis^{15,d} , V. Gibson⁵³ , H.K. Giemza³⁹ , A.L. Gilman⁶¹ , M. Giovannetti²⁵ , A. Gioventù⁴³ , P. Gironella Gironell⁴³ , C. Giugliano^{23,j} , M.A. Giza³⁸ , E.L. Gkougkousis⁵⁹ , F.C. Glaser^{13,19} , V.V. Gligorov¹⁵ , C. Göbel⁶⁷ , E. Golobardes⁴² , D. Golubkov⁴¹ , A. Golutvin^{59,41,46} , A. Gomes^{2,a,\dagger} , S. Gomez Fernandez⁴³ , F. Goncalves Abrantes⁶¹ , M. Goncerz³⁸ , G. Gong⁴ , J. A. Gooding¹⁷ , I.V. Gorelov⁴¹ , C. Gotti²⁸ , J.P. Grabowski⁷³ , L.A. Granado Cardoso⁴⁶ , E. Graugés⁴³ , E. Graverini⁴⁷ , L. Grazette⁵⁴ , G. Graziani , A. T. Grecu⁴⁰ , L.M. Greeven³⁵ , N.A. Grieser⁶³ , L. Grillo⁵⁷ , S. Gromov⁴¹ , C. Gu¹⁴ , M. Guarise²³ , M. Guittiere¹³ , V. Guliaeva⁴¹ , P. A. Günther¹⁹ , A.-K. Guseinov⁴¹ , E. Gushchin⁴¹ , Y. Guz^{6,41,46} , T. Gys⁴⁶ , T. Hadavizadeh¹ , C. Hadjivassiliou⁶⁴ , G. Haefeli⁴⁷ , C. Haen⁴⁶ , J. Haimberger⁴⁶ , M. Hajheidari⁴⁶ , T. Halewood-leagas⁵⁸ , M.M. Halvorsen⁴⁶ , P.M. Hamilton⁶⁴ , J. Hammerich⁵⁸ , Q. Han⁸ , X. Han¹⁹ , S. Hansmann-Menzemer¹⁹ , L. Hao⁷ , N. Harnew⁶¹ , T. Harrison⁵⁸ , M. Hartmann¹³ , C. Hasse⁴⁶ , J. He^{7,c} , K. Heijhoff³⁵ , F. Hemmer⁴⁶ , C. Henderson⁶³ , R.D.L. Henderson^{1,54} , A.M. Hennequin⁴⁶ , K. Hennessy⁵⁸ , L. Henry⁴⁷ , J. Herd⁵⁹ , J. Heuel¹⁶ , A. Hicheur³ , D. Hill⁴⁷ , S.E. Hollitt¹⁷ , J. Horswill⁶⁰ , R. Hou⁸ , Y. Hou¹⁰ , N. Howarth⁵⁸ , J. Hu¹⁹ , J. Hu⁶⁹ , W. Hu⁶ , X. Hu⁴ , W. Huang⁷ , W. Hulsbergen³⁵ , R.J. Hunter⁵⁴ , M. Hushchyn⁴¹ , D. Hutchcroft⁵⁸ , M. Idzik³⁷ , D. Ilin⁴¹ , P. Ilten⁶³ , A. Inglessi⁴¹ , A. Iniuksin⁴¹ , A. Ishteev⁴¹ , K. Ivshin⁴¹ , R. Jacobsson⁴⁶ , H. Jage¹⁶ , S.J. Jaimes Elles^{45,72} , S. Jakobsen⁴⁶ , E. Jans³⁵ , B.K. Jashal⁴⁵ , A. Jawahery⁶⁴ , V. Jevtic¹⁷ , E. Jiang⁶⁴ , X. Jiang^{5,7} , Y. Jiang⁷ , Y. J. Jiang⁶ , M. John⁶¹ , D. Johnson⁵¹ , C.R. Jones⁵³ , T.P. Jones⁵⁴ , S. Joshi³⁹ , B. Jost⁴⁶ , N. Jurik⁴⁶ , I. Juszczak³⁸ , D. Kaminaris⁴⁷ , S. Kandybei⁴⁹ , Y. Kang⁴ , M. Karacson⁴⁶ , D. Karpenkov⁴¹ , M. Karpov⁴¹ , A. M. Kauniskangas⁴⁷ , J.W. Kautz⁶³ , F. Keizer⁴⁶ , D.M. Keller⁶⁶ , M. Kenzie⁵³ , T. Ketel³⁵ , B. Khanji⁶⁶ , A. Kharisova⁴¹ , S. Kholodenko³² , G. Khreich¹³ , T. Kirn¹⁶ , V.S. Kirsebom⁴⁷ , O. Kitouni⁶² , S. Klaver³⁶ , N. Kleijne^{32,q} ,

K. Klimaszewski³⁹ [ID](#), M.R. Kmiec³⁹ [ID](#), S. Kolliiev⁵⁰ [ID](#), L. Kolk¹⁷ [ID](#), A. Konoplyannikov⁴¹ [ID](#),
 P. Kopciewicz^{37,46} [ID](#), P. Koppenburg³⁵ [ID](#), M. Korolev⁴¹ [ID](#), I. Kostiuk³⁵ [ID](#), O. Kot⁵⁰,
 S. Kotriakhova [ID](#), A. Kozachuk⁴¹ [ID](#), P. Kravchenko⁴¹ [ID](#), L. Kravchuk⁴¹ [ID](#), M. Kreps⁵⁴ [ID](#),
 S. Kretzschmar¹⁶ [ID](#), P. Krokovny⁴¹ [ID](#), W. Krupa⁶⁶ [ID](#), W. Krzemien³⁹ [ID](#), J. Kubat¹⁹,
 S. Kubis⁷⁷ [ID](#), W. Kucewicz³⁸ [ID](#), M. Kucharczyk³⁸ [ID](#), V. Kudryavtsev⁴¹ [ID](#), E. Kulikova⁴¹ [ID](#),
 A. Kupsc⁷⁸ [ID](#), B. K. Kutsenko¹² [ID](#), D. Lacarrere⁴⁶ [ID](#), G. Lafferty⁶⁰ [ID](#), A. Lai²⁹ [ID](#),
 A. Lampis²⁹ [ID](#), D. Lancierini⁴⁸ [ID](#), C. Landesa Gomez⁴⁴ [ID](#), J.J. Lane¹ [ID](#), R. Lane⁵² [ID](#),
 C. Langenbruch¹⁹ [ID](#), J. Langer¹⁷ [ID](#), O. Lantwin⁴¹ [ID](#), T. Latham⁵⁴ [ID](#), F. Lazzari^{32,r} [ID](#),
 C. Lazzeroni⁵¹ [ID](#), R. Le Gac¹² [ID](#), S.H. Lee⁷⁹ [ID](#), R. Lefèvre¹¹ [ID](#), A. Leflat⁴¹ [ID](#), S. Legotin⁴¹ [ID](#),
 M. Lehuraux⁵⁴ [ID](#), O. Leroy¹² [ID](#), T. Lesiak³⁸ [ID](#), B. Leverington¹⁹ [ID](#), A. Li⁴ [ID](#), H. Li⁶⁹ [ID](#),
 K. Li⁸ [ID](#), L. Li⁶⁰ [ID](#), P. Li⁴⁶ [ID](#), P.-R. Li⁷⁰ [ID](#), S. Li⁸ [ID](#), T. Li⁵ [ID](#), T. Li⁶⁹ [ID](#), Y. Li⁸, Y. Li⁵ [ID](#),
 Z. Li⁶⁶ [ID](#), Z. Lian⁴ [ID](#), X. Liang⁶⁶ [ID](#), C. Lin⁷ [ID](#), T. Lin⁵⁵ [ID](#), R. Lindner⁴⁶ [ID](#), V. Lisovskyi⁴⁷ [ID](#),
 R. Litvinov^{29,i} [ID](#), G. Liu⁶⁹ [ID](#), H. Liu⁷ [ID](#), K. Liu⁷⁰ [ID](#), Q. Liu⁷ [ID](#), S. Liu^{5,7} [ID](#), Y. Liu⁵⁶ [ID](#),
 Y. Liu⁷⁰, Y. L. Liu⁵⁹ [ID](#), A. Lobo Salvia⁴³ [ID](#), A. Loi²⁹ [ID](#), J. Lomba Castro⁴⁴ [ID](#), T. Long⁵³ [ID](#),
 J.H. Lopes³ [ID](#), A. Lopez Huertas⁴³ [ID](#), S. López Solino⁴⁴ [ID](#), G.H. Lovell⁵³ [ID](#), C. Lucarelli^{24,k} [ID](#),
 D. Lucchesi^{30,o} [ID](#), S. Luchuk⁴¹ [ID](#), M. Lucio Martinez⁷⁶ [ID](#), V. Lukashenko^{35,50} [ID](#), Y. Luo⁴ [ID](#),
 A. Lupato³⁰ [ID](#), E. Luppi^{23,j} [ID](#), K. Lynch²⁰ [ID](#), X.-R. Lyu⁷ [ID](#), G. M. Ma⁴ [ID](#), R. Ma⁷ [ID](#),
 S. Maccolini¹⁷ [ID](#), F. Machefert¹³ [ID](#), F. Maciuc⁴⁰ [ID](#), I. Mackay⁶¹ [ID](#), L.R. Madhan Mohan⁵³ [ID](#),
 M. M. Madurai⁵¹ [ID](#), A. Maevskiy⁴¹ [ID](#), D. Magdalinski³⁵ [ID](#), D. Maisuzenko⁴¹ [ID](#),
 M.W. Majewski³⁷, J.J. Malczewski³⁸ [ID](#), S. Malde⁶¹ [ID](#), B. Malecki^{38,46} [ID](#), L. Malentacca⁴⁶,
 A. Malinin⁴¹ [ID](#), T. Maltsev⁴¹ [ID](#), G. Manca^{29,i} [ID](#), G. Mancinelli¹² [ID](#), C. Mancuso^{27,13,m} [ID](#),
 R. Manera Escalero⁴³, D. Manuzzi²² [ID](#), D. Marangotto^{27,m} [ID](#), J.F. Marchand¹⁰ [ID](#),
 R. Marchevski⁴⁷ [ID](#), U. Marconi²² [ID](#), S. Mariani⁴⁶ [ID](#), C. Marin Benito^{43,46} [ID](#), J. Marks¹⁹ [ID](#),
 A.M. Marshall⁵² [ID](#), P.J. Marshall⁵⁸, G. Martelli^{31,p} [ID](#), G. Martellotti³³ [ID](#), L. Martinazzoli⁴⁶ [ID](#),
 M. Martinelli^{28,n} [ID](#), D. Martinez Santos⁴⁴ [ID](#), F. Martinez Vidal⁴⁵ [ID](#), A. Massafferri² [ID](#),
 M. Materok¹⁶ [ID](#), R. Matev⁴⁶ [ID](#), A. Mathad⁴⁸ [ID](#), V. Matiunin⁴¹ [ID](#), C. Matteuzzi^{66,28} [ID](#),
 K.R. Mattioli¹⁴ [ID](#), A. Mauri⁵⁹ [ID](#), E. Maurice¹⁴ [ID](#), J. Mauricio⁴³ [ID](#), M. Mazurek⁴⁶ [ID](#),
 M. McCann⁵⁹ [ID](#), L. McConnell²⁰ [ID](#), T.H. McGrath⁶⁰ [ID](#), N.T. McHugh⁵⁷ [ID](#), A. McNab⁶⁰ [ID](#),
 R. McNulty²⁰ [ID](#), B. Meadows⁶³ [ID](#), G. Meier¹⁷ [ID](#), D. Melnychuk³⁹ [ID](#), M. Merk^{35,76} [ID](#),
 A. Merli^{27,m} [ID](#), L. Meyer Garcia³ [ID](#), D. Miao^{5,7} [ID](#), H. Miao⁷ [ID](#), M. Mikhaseko^{73,e} [ID](#),
 D.A. Milanes⁷² [ID](#), A. Minotti^{28,n} [ID](#), E. Minucci⁶⁶ [ID](#), T. Miralles¹¹ [ID](#), S.E. Mitchell⁵⁶ [ID](#),
 B. Mitreska¹⁷ [ID](#), D.S. Mitzel¹⁷ [ID](#), A. Modak⁵⁵ [ID](#), A. Mödden¹⁷ [ID](#), R.A. Mohammed⁶¹ [ID](#),
 R.D. Moise¹⁶ [ID](#), S. Mokhnenko⁴¹ [ID](#), T. Mombächer⁴⁶ [ID](#), M. Monk^{54,1} [ID](#), I.A. Monroy⁷² [ID](#),
 S. Monteil¹¹ [ID](#), A. Morcillo Gomez⁴⁴ [ID](#), G. Morello²⁵ [ID](#), M.J. Morello^{32,q} [ID](#),
 M.P. Morgenthaler¹⁹ [ID](#), J. Moron³⁷ [ID](#), A.B. Morris⁴⁶ [ID](#), A.G. Morris¹² [ID](#), R. Mountain⁶⁶ [ID](#),
 H. Mu⁴ [ID](#), Z. M. Mu⁶ [ID](#), E. Muhammad⁵⁴ [ID](#), F. Muheim⁵⁶ [ID](#), M. Mulder⁷⁵ [ID](#), K. Müller⁴⁸ [ID](#),
 F. Múnoz-Rojas⁹ [ID](#), R. Murta⁵⁹ [ID](#), P. Naik⁵⁸ [ID](#), T. Nakada⁴⁷ [ID](#), R. Nandakumar⁵⁵ [ID](#),
 T. Nanut⁴⁶ [ID](#), I. Nasteva³ [ID](#), M. Needham⁵⁶ [ID](#), N. Neri^{27,m} [ID](#), S. Neubert⁷³ [ID](#), N. Neufeld⁴⁶ [ID](#),
 P. Neustroev⁴¹, R. Newcombe⁵⁹, J. Nicolini^{17,13} [ID](#), D. Nicotra⁷⁶ [ID](#), E.M. Niel⁴⁷ [ID](#),
 N. Nikitin⁴¹ [ID](#), P. Nogga⁷³, N.S. Nolte⁶² [ID](#), C. Normand^{10,i,29} [ID](#), J. Novoa Fernandez⁴⁴ [ID](#),
 G. Nowak⁶³ [ID](#), C. Nunez⁷⁹ [ID](#), H. N. Nur⁵⁷ [ID](#), A. Oblakowska-Mucha³⁷ [ID](#), V. Obraztsov⁴¹ [ID](#),
 T. Oeser¹⁶ [ID](#), S. Okamura^{23,j,46} [ID](#), R. Oldeman^{29,i} [ID](#), F. Oliva⁵⁶ [ID](#), M. Olocco¹⁷ [ID](#),
 C.J.G. Onderwater⁷⁶ [ID](#), R.H. O’Neil⁵⁶ [ID](#), J.M. Otalora Goicochea³ [ID](#), T. Ovsiannikova⁴¹ [ID](#),
 P. Owen⁴⁸ [ID](#), A. Oyanguren⁴⁵ [ID](#), O. Ozcelik⁵⁶ [ID](#), K.O. Paddeken⁷³ [ID](#), B. Pagare⁵⁴ [ID](#),
 P.R. Pais¹⁹ [ID](#), T. Pajero⁶¹ [ID](#), A. Palano²¹ [ID](#), M. Palutan²⁵ [ID](#), G. Panshin⁴¹ [ID](#), L. Paolucci⁵⁴ [ID](#),
 A. Papanestis⁵⁵ [ID](#), M. Pappagallo^{21,g} [ID](#), L.L. Pappalardo^{23,j} [ID](#), C. Pappenheimer⁶³ [ID](#),
 C. Parkes⁶⁰ [ID](#), B. Passalacqua^{23,j} [ID](#), G. Passaleva²⁴ [ID](#), D. Passaro^{32,q} [ID](#), A. Pastore²¹ [ID](#),
 M. Patel⁵⁹ [ID](#), J. Patoc⁶¹ [ID](#), C. Patrignani^{22,h} [ID](#), C.J. Pawley⁷⁶ [ID](#), A. Pellegrino³⁵ [ID](#),
 M. Pepe Altarelli²⁵ [ID](#), S. Perazzini²² [ID](#), D. Pereima⁴¹ [ID](#), A. Pereiro Castro⁴⁴ [ID](#), P. Perret¹¹ [ID](#),
 A. Perro⁴⁶ [ID](#), K. Petridis⁵² [ID](#), A. Petrolini^{26,l} [ID](#), S. Petrucci⁵⁶ [ID](#), H. Pham⁶⁶ [ID](#), L. Pica^{32,q} [ID](#),

E.J. Walton¹ , G. Wan⁶ , C. Wang¹⁹ , G. Wang⁸ , J. Wang⁶ , J. Wang⁵ , J. Wang⁴ ,
 J. Wang⁷¹ , M. Wang²⁷ , N. W. Wang⁷ , R. Wang⁵² , X. Wang⁶⁹ , X. W. Wang⁵⁹ ,
 Y. Wang⁸ , Z. Wang¹³ , Z. Wang⁴ , Z. Wang⁷ , J.A. Ward^{54,1} , N.K. Watson⁵¹ ,
 D. Websdale⁵⁹ , Y. Wei⁶ , B.D.C. Westhenry⁵² , D.J. White⁶⁰ , M. Whitehead⁵⁷ ,
 A.R. Wiederhold⁵⁴ , D. Wiedner¹⁷ , G. Wilkinson⁶¹ , M.K. Wilkinson⁶³ ,
 M. Williams⁶² , M.R.J. Williams⁵⁶ , R. Williams⁵³ , F.F. Wilson⁵⁵ , W. Wislicki³⁹ ,
 M. Witek³⁸ , L. Witola¹⁹ , C.P. Wong⁶⁵ , G. Wormser¹³ , S.A. Wotton⁵³ , H. Wu⁶⁶ ,
 J. Wu⁸ , Y. Wu⁶ , K. Wyllie⁴⁶ , S. Xian⁶⁹ , Z. Xiang⁵ , Y. Xie⁸ , A. Xu³² , J. Xu⁷ ,
 L. Xu⁴ , L. Xu⁴ , M. Xu⁵⁴ , Z. Xu¹¹ , Z. Xu⁷ , Z. Xu⁵ , D. Yang⁴ , S. Yang⁷ ,
 X. Yang⁶ , Y. Yang^{26,l} , Z. Yang⁶ , V. Yeroshenko¹³ , H. Yeung⁶⁰ ,
 H. Yin⁸ , C. Y. Yu⁶ , J. Yu⁶⁸ , X. Yuan⁵ , E. Zaffaroni⁴⁷ , M. Zavertyaev¹⁸ ,
 M. Zdybal³⁸ , M. Zeng⁴ , C. Zhang⁶ , D. Zhang⁸ , J. Zhang⁷ , L. Zhang⁴ ,
 S. Zhang⁶⁸ , S. Zhang⁶ , Y. Zhang⁶ , Y. Zhang⁶¹ , Y. Z. Zhang⁴ , Y. Zhao¹⁹ ,
 A. Zharkova⁴¹ , A. Zhelezov¹⁹ , X. Z. Zheng⁴ , Y. Zheng⁷ , T. Zhou⁶ , X. Zhou⁸ ,
 Y. Zhou⁷ , V. Zhovkovska¹³ , L. Z. Zhu⁷ , X. Zhu⁴ , X. Zhu⁸ , Z. Zhu⁷ ,
 V. Zhukov^{16,41} , J. Zhuo⁴⁵ , Q. Zou^{5,7} , D. Zuliani³⁰ , G. Zunică⁶⁰

¹*School of Physics and Astronomy, Monash University, Melbourne, Australia*

²*Centro Brasileiro de Pesquisas Físicas (CBPF), Rio de Janeiro, Brazil*

³*Universidade Federal do Rio de Janeiro (UFRJ), Rio de Janeiro, Brazil*

⁴*Center for High Energy Physics, Tsinghua University, Beijing, China*

⁵*Institute Of High Energy Physics (IHEP), Beijing, China*

⁶*School of Physics State Key Laboratory of Nuclear Physics and Technology, Peking University, Beijing, China*

⁷*University of Chinese Academy of Sciences, Beijing, China*

⁸*Institute of Particle Physics, Central China Normal University, Wuhan, Hubei, China*

⁹*Consejo Nacional de Rectores (CONARE), San Jose, Costa Rica*

¹⁰*Université Savoie Mont Blanc, CNRS, IN2P3-LAPP, Annecy, France*

¹¹*Université Clermont Auvergne, CNRS/IN2P3, LPC, Clermont-Ferrand, France*

¹²*Aix Marseille Univ, CNRS/IN2P3, CPPM, Marseille, France*

¹³*Université Paris-Saclay, CNRS/IN2P3, IJCLab, Orsay, France*

¹⁴*Laboratoire Leprince-Ringuet, CNRS/IN2P3, Ecole Polytechnique, Institut Polytechnique de Paris, Palaiseau, France*

¹⁵*LPNHE, Sorbonne Université, Paris Diderot Sorbonne Paris Cité, CNRS/IN2P3, Paris, France*

¹⁶*I. Physikalisches Institut, RWTH Aachen University, Aachen, Germany*

¹⁷*Fakultät Physik, Technische Universität Dortmund, Dortmund, Germany*

¹⁸*Max-Planck-Institut für Kernphysik (MPIK), Heidelberg, Germany*

¹⁹*Physikalisch Institut, Ruprecht-Karls-Universität Heidelberg, Heidelberg, Germany*

²⁰*School of Physics, University College Dublin, Dublin, Ireland*

²¹*INFN Sezione di Bari, Bari, Italy*

²²*INFN Sezione di Bologna, Bologna, Italy*

²³*INFN Sezione di Ferrara, Ferrara, Italy*

²⁴*INFN Sezione di Firenze, Firenze, Italy*

²⁵*INFN Laboratori Nazionali di Frascati, Frascati, Italy*

²⁶*INFN Sezione di Genova, Genova, Italy*

²⁷*INFN Sezione di Milano, Milano, Italy*

²⁸*INFN Sezione di Milano-Bicocca, Milano, Italy*

²⁹*INFN Sezione di Cagliari, Monserrato, Italy*

³⁰*Università degli Studi di Padova, Università e INFN, Padova, Padova, Italy*

³¹*INFN Sezione di Perugia, Perugia, Italy*

³²*INFN Sezione di Pisa, Pisa, Italy*

³³*INFN Sezione di Roma La Sapienza, Roma, Italy*

³⁴*INFN Sezione di Roma Tor Vergata, Roma, Italy*

³⁵*Nikhef National Institute for Subatomic Physics, Amsterdam, Netherlands*

³⁶*Nikhef National Institute for Subatomic Physics and VU University Amsterdam, Amsterdam,*

Netherlands

³⁷AGH - University of Science and Technology, Faculty of Physics and Applied Computer Science, Kraków, Poland

³⁸Henryk Niewodniczanski Institute of Nuclear Physics Polish Academy of Sciences, Kraków, Poland

³⁹National Center for Nuclear Research (NCBJ), Warsaw, Poland

⁴⁰Horia Hulubei National Institute of Physics and Nuclear Engineering, Bucharest-Magurele, Romania

⁴¹Affiliated with an institute covered by a cooperation agreement with CERN

⁴²DS4DS, La Salle, Universitat Ramon Llull, Barcelona, Spain

⁴³ICCUB, Universitat de Barcelona, Barcelona, Spain

⁴⁴Instituto Galego de Física de Altas Enerxías (IGFAE), Universidade de Santiago de Compostela, Santiago de Compostela, Spain

⁴⁵Instituto de Fisica Corpuscular, Centro Mixto Universidad de Valencia - CSIC, Valencia, Spain

⁴⁶European Organization for Nuclear Research (CERN), Geneva, Switzerland

⁴⁷Institute of Physics, Ecole Polytechnique Fédérale de Lausanne (EPFL), Lausanne, Switzerland

⁴⁸Physik-Institut, Universität Zürich, Zürich, Switzerland

⁴⁹NSC Kharkiv Institute of Physics and Technology (NSC KIPT), Kharkiv, Ukraine

⁵⁰Institute for Nuclear Research of the National Academy of Sciences (KINR), Kyiv, Ukraine

⁵¹University of Birmingham, Birmingham, United Kingdom

⁵²H.H. Wills Physics Laboratory, University of Bristol, Bristol, United Kingdom

⁵³Cavendish Laboratory, University of Cambridge, Cambridge, United Kingdom

⁵⁴Department of Physics, University of Warwick, Coventry, United Kingdom

⁵⁵STFC Rutherford Appleton Laboratory, Didcot, United Kingdom

⁵⁶School of Physics and Astronomy, University of Edinburgh, Edinburgh, United Kingdom

⁵⁷School of Physics and Astronomy, University of Glasgow, Glasgow, United Kingdom

⁵⁸Oliver Lodge Laboratory, University of Liverpool, Liverpool, United Kingdom

⁵⁹Imperial College London, London, United Kingdom

⁶⁰Department of Physics and Astronomy, University of Manchester, Manchester, United Kingdom

⁶¹Department of Physics, University of Oxford, Oxford, United Kingdom

⁶²Massachusetts Institute of Technology, Cambridge, MA, United States

⁶³University of Cincinnati, Cincinnati, OH, United States

⁶⁴University of Maryland, College Park, MD, United States

⁶⁵Los Alamos National Laboratory (LANL), Los Alamos, NM, United States

⁶⁶Syracuse University, Syracuse, NY, United States

⁶⁷Pontifícia Universidade Católica do Rio de Janeiro (PUC-Rio), Rio de Janeiro, Brazil, associated to ³

⁶⁸School of Physics and Electronics, Hunan University, Changsha City, China, associated to ⁸

⁶⁹Guangdong Provincial Key Laboratory of Nuclear Science, Guangdong-Hong Kong Joint Laboratory of Quantum Matter, Institute of Quantum Matter, South China Normal University, Guangzhou, China, associated to ⁴

⁷⁰Lanzhou University, Lanzhou, China, associated to ⁵

⁷¹School of Physics and Technology, Wuhan University, Wuhan, China, associated to ⁴

⁷²Departamento de Fisica , Universidad Nacional de Colombia, Bogota, Colombia, associated to ¹⁵

⁷³Universität Bonn - Helmholtz-Institut für Strahlen und Kernphysik, Bonn, Germany, associated to ¹⁹

⁷⁴Eotvos Lorand University, Budapest, Hungary, associated to ⁴⁶

⁷⁵Van Swinderen Institute, University of Groningen, Groningen, Netherlands, associated to ³⁵

⁷⁶Universiteit Maastricht, Maastricht, Netherlands, associated to ³⁵

⁷⁷Tadeusz Kosciuszko Cracow University of Technology, Cracow, Poland, associated to ³⁸

⁷⁸Department of Physics and Astronomy, Uppsala University, Uppsala, Sweden, associated to ⁵⁷

⁷⁹University of Michigan, Ann Arbor, MI, United States, associated to ⁶⁶

⁸⁰Departement de Physique Nucléaire (SPhN), Gif-Sur-Yvette, France

^aUniversidade de Brasília, Brasília, Brazil

^bCentro Federal de Educacão Tecnológica Celso Suckow da Fonseca, Rio De Janeiro, Brazil

^cHangzhou Institute for Advanced Study, UCAS, Hangzhou, China

^dLIP6, Sorbonne Universite, Paris, France

^eExcellence Cluster ORIGINS, Munich, Germany

^fUniversidad Nacional Autónoma de Honduras, Tegucigalpa, Honduras

^gUniversità di Bari, Bari, Italy

^h Università di Bologna, Bologna, Italy
ⁱ Università di Cagliari, Cagliari, Italy
^j Università di Ferrara, Ferrara, Italy
^k Università di Firenze, Firenze, Italy
^l Università di Genova, Genova, Italy
^m Università degli Studi di Milano, Milano, Italy
ⁿ Università di Milano Bicocca, Milano, Italy
^o Università di Padova, Padova, Italy
^p Università di Perugia, Perugia, Italy
^q Scuola Normale Superiore, Pisa, Italy
^r Università di Pisa, Pisa, Italy
^s Università della Basilicata, Potenza, Italy
^t Università di Roma Tor Vergata, Roma, Italy
^u Università di Siena, Siena, Italy
^v Università di Urbino, Urbino, Italy
^w Universidad de Alcalá, Alcalá de Henares , Spain
^x Universidade da Coruña, Coruña, Spain
^y Department of Physics/Division of Particle Physics, Lund, Sweden

† Deceased